Estimating the Effectiveness of Stone Columns in Mitigating Post-Liquefaction Settlement Using Plaxis 2D

Roisha Maharjan

Thesis submitted to the Faculty of the Virginia Polytechnic Institute and State University in partial fulfillment of the requirements for the degree of

Master of Science

in

Civil Engineering

Adrian Rodriguez-Marek, Chair

Alba Yerro-Colom, Chair

Russell A. Green

December 7, 2023

Blacksburg, VA

Keywords: Post-liquefaction settlement, Stone Columns, Earthquake, Plaxis 2D

Estimating the Effectiveness of Stone Columns in Mitigating Post-Liquefaction Settlement Using Plaxis 2D

Roisha Maharjan

ABSTRACT

When the excess pore water pressure generated during an earthquake dissipates in saturated loose sand, it causes post-liquefaction reconsolidation that can potentially yield substantial damage to the structure. To build resilient infrastructure, it is paramount to estimate these settlements as well as introduce soil reinforcement techniques to mitigate associated risks. Although there are abundant studies on liquefaction triggering assessment, the study of post-liquefaction settlement and the effects of stone columns as soil reinforcement is a relatively less established field. Generally, simplified empirical methods are employed for settlement evaluations. However, they possess several limitations such as the influence of non-liquefiable layers, soil fabric, permeability, and so on. Numerical models can be utilized to capture these effects with proper validation. This study evaluates the performance of stone columns in reducing seismically induced post-liquefaction settlement utilizing the Finite Element Method (FEM) and constitutive relationship, PM4Sand model, as it has been extended to account for reconsolidation settlement. The ability of the numerical framework to capture reconsolidation settlement is validated by replicating a shake table test performed on Ottawa F-55 sand. Results are compared with a previous numerical study inspired by the same experiment. After validation, a generic numerical model is proposed, and the performance of the natural ground and the reinforced ground is compared. A parametric analysis using 12 different ground motions is performed to assess the effect of varying ground motion intensity on the post-liquefaction settlement. The analysis is also performed with the conventional PM4Sand model (without the extension for reconsolidation). Finally, simulations are performed with a footing load above the soil model. The results demonstrate that (a) the presence of stone columns reduces post-liquefaction settlement, and (b) conventional constitutive models can highly underpredict post-liquefaction settlement. Further research is required to assess the effects of (a) 3D, (b) variations in permeability, (c) parametric analysis of stone columns, and (d) densification of stone columns.

Estimating the Effectiveness of Stone Columns in Mitigating Post-Liquefaction Settlement Using Plaxis 2D

Roisha Maharjan

GENERAL AUDIENCE ABSTRACT

When subjected to an earthquake, loose saturated sand may undergo liquefaction and exhibit a reduction in shear strength due to a rise in excess pore water pressure and the corresponding reduction in effective stress. This leads to failures associated with settlements resulting from the gradual dissipation of excess pore pressures. This mechanism results in post-liquefaction settlement. Several authors have investigated the mechanism of the post-liquefaction behavior of sand and proposed methodologies to assess the deformation caused by seismic loads. They mainly conclude that the reconsolidation mechanism is characterized by a decrease in the overall soil stiffness and an increase in permeability. Among different methodologies to quantify this settlement, finite element numerical modeling is the most widely used. The primary task in performing such numerical simulation is to select the best constitutive model (i.e., stress-strain relationships) that can accurately capture post-liquefaction behavior. In this study, the capabilities and limitations of the most common constitutive models are reviewed. Moreover, the efficacy of stone columns is also assessed to mitigate the risk posed by liquefaction. Firstly, the numerical framework is validated against data from a shake table test experiment. Then, a numerical model is proposed and subjected to different seismic motions. The settlement of the ground with and without stone columns is assessed and compared for all motions. In addition, the efficacy of stone columns is also analyzed by simulating the model with a footing load. Thus, this study provides insights into the effectiveness of stone columns under different seismic motions.

ACKNOWLEDGMENTS

I would like to thank my advisors, Dr. Alba Yerro-Colom and Dr. Adrian Rodriguez-Marek, for their motivation and continuous support throughout my journey at Virginia Tech. I am deeply indebted to both for being excellent advisors, and I am immensely grateful for their valuable feedback and unwavering guidance throughout the course of my research. Their expertise and encouragement have been extremely significant in shaping this work.

I am also deeply thankful to Dr. Russell Green for serving on my thesis review committee and dedicating time to reviewing this research. His valuable assistance and insights during my coursework at university greatly refined my journey. I also appreciate Dr. Yerro-Colom's research group for providing constructive feedback on my thesis, which has significantly enhanced the quality of this research.

I would like to acknowledge the friendship and encouragement of two special friends, Sanish Bhochhibhoya and Samiksha Thapa, for their support in providing me with laptops for analysis purposes, which facilitated the progress of this work. I am truly grateful for their kindness.

Finally, I would like to show appreciation to my family and friends in Nepal for their constant encouragement, understanding, and patience. Their guidance has been a constant source of motivation throughout this journey.

Table of Contents

List of Figures

List of Tables

Chapter 1

Introduction

1.1 Motivation

Liquefaction of saturated sand triggered by earthquakes is one of the major causes of seismic damage to infrastructures and superstructures (Green and Bommer 2019). When subjected to an earthquake, loose saturated sand can undergo liquefaction; if it does, it experiences a significant loss in shear strength due to an increase in excess pore pressure and a corresponding reduction in effective stress. After an earthquake, reconsolidation occurs when the excess pore pressure gradually dissipates, resulting in post-liquefaction (reconsolidation) settlement. There have been several case histories in past earthquakes with severe liquefaction-induced settlements, e.g., Niigata ($M_w = 7.6$) in 1964, Kobe ($M_w = 6.9$) in 1995, Chile ($M_w = 8.8$) in 2010, Christchurch ($M_w = 6.2$) in 2011, Loma Prieta ($M_w = 6.9$) in 1989 (Rashidian and Baise 2020).

Despite extensive efforts made in the geotechnical and civil engineering fields to predict earthquake hazards and minimize liquefaction-related losses, there is a need to better understand these mechanisms, particularly liquefaction-induced settlement. Most studies in this field are predominantly focused on liquefaction triggering and residual strength, leaving the reconsolidation mechanism understudied. Moreover, there is a limited understanding of the effectiveness of ground improvement techniques in mitigating reconsolidation settlement. This highlights the importance of a comprehensive study on post-liquefaction behavior and the potential benefits of soil reinforcement methods in reducing associated risks to infrastructure stability (Wu and Seed 2004).

Generally, construction sites with shallow liquefiable soil layers entail the installation of deep foundations or ground improvement techniques to mitigate the impact of soil liquefaction. Deep foundations might not be feasible due to the high cost and extensive construction equipment (Thum et al. 2022). Several mitigation techniques that lead to ground densification and increased drainage have been developed to prevent liquefaction potential and minimize

associated damage (Zhou et al. 2021). Among these, stone columns are a cost-effective approach that enhances soil density through vibration and replacement, increases lateral stress, and reduces shear stress by introducing rigid elements (Martin and Martin 1992).

The efficacy of stone columns has been observed in past earthquakes (Iai et al. 1988; Li et al. 2018). Moreover, full-scale tests have been conducted to verify that stone columns increase the relative density of surrounding ground and prevent the generation of excess pore pressures, concurrently providing shear reinforcement. Apart from experimental studies, numerical simulations may be utilized to compare the evolution of excess pore pressures (generation and dissipation) and deformations of natural ground and reinforced ground with stone columns.

1.2 Research Objectives

The main objectives of this research are presented below:

- Review different constitutive models that can capture liquefaction-induced settlement and identify how these models address the post-liquefaction behavior of soil. This will provide insights into the capabilities and limitations of each constitutive model.
- Create and validate a numerical framework that can successfully capture liquefaction triggering and post-liquefaction settlement by utilizing the modified PM4Sand model (advanced constitutive model) developed by Ziotopoulou and Boulanger (2017).
- Perform a parametric analysis with a wide range of ground motion intensities to comprehend the influence of stone columns on mitigating liquefaction.

1.3 Organization

This study is organized into six sections:

- The second chapter outlines a background study of the main topics of research: liquefaction, post-liquefaction mechanism, stone column as a mitigation measure, and constitutive modeling.
- The third chapter comprises the material and methodology implemented to achieve the main goals of the research. Therefore, a brief description of the steps utilized to analyze the model with and without stone columns in Plaxis 2D (Plaxis 2018) is explained. At first, it consists of the validation of the numerical framework using the PM4Sand model

in which the shake table test experiment by Thevanayagam et al. (2009) was replicated in Plaxis 2D. The results in terms of excess pore pressure and settlement from Plaxis 2D were compared with the experiment as well as the previous study performed in FLAC (Itasca Consulting Group 2016) by Basu et al. (2022).

- The fourth chapter presents a new numerical model proposed to study the effects of stone columns in natural ground. It presents parametric analysis to understand the influence of stone columns when subjected to twelve different input motions of a wide range of magnitude and Arias Intensity. In addition, the post-liquefaction settlement using an extended version of PM4Sand was compared with the conventional one. Finally, the numerical model with footing was analyzed to capture the effects of stone columns under the surcharge load of the foundation.
- The fifth chapter presents the conclusions and summary of this research along with limitations and recommendations for future work.

Chapter 2

Background Study

2.1 Liquefaction

During an earthquake, the stresses and deformation in the ground can disturb the soil structure, specifically in saturated, geologically unconsolidated soils. As a result, saturated sand might tend to contract such that there is a transfer of overburden stress from the soil skeleton to pore fluid under undrained conditions (Kramer and Seed 1988). Consequently, the pore pressure builds up, and the shear strength of the soil decreases (Seed et al. 1983). If there is a complete transfer of overburden from the soil skeleton to the pore fluid, this phenomenon is referred to as initial liquefaction or liquefaction triggering; if such transfer is partial, then the phenomenon is referred to as partial liquefaction. There are two related phenomena associated with the occurrence of liquefaction: flow liquefaction and cyclic mobility (Kramer 1996). Flow liquefaction occurs when the shear stress required for the static equilibrium of a soil mass exceeds the in-situ shear strength of soil in its liquefied steady form. The large deformations generated by flow liquefaction are produced by the static shear stresses. Cyclic mobility occurs when the soil's dilative tendencies prevent large deformations following shaking, but limited deformations can occur during shaking. Failures due to cyclic mobility progress gradually during earthquake shaking and are driven by both cyclic and static shear stresses. A special case of cyclic mobility is level-ground liquefaction, which can yield large movements during seismic events, leading to ground surface settlements, bearing capacity failure of foundations, and permanent displacements (Toloza 2018).

A simplified assessment of liquefaction-induced ground settlement remains a highly valuable tool for assessing liquefaction triggering or preliminary assessments. Bray and Macedo (2017) proposed a combination of three components to assess liquefaction-induced ground settlement: (a) settlement due to the initiation of sediment ejecta, (b) strain resulting from pre-existing shear stresses, and (c) reconsolidation settlement caused by volumetric consolidation. Generally, in many scenarios, the approach for estimating ground settlement due to liquefaction relies on empirical techniques (Cetin et al. 2004; Ishihara and Yoshimine 1992; Jiang et al.

2021; Tokimatsu and Seed 1987; Zhang et al. 2010). These models are based on geotechnical tests such as the SPT (Standard Penetration Test), the CPT (Cone Penetration Test), or the Shear wave velocity profile (V_S). These simplified approaches correlate the volumetric strains resulting from the dissipation of pore-water pressures through simple charts with relative density (D_r) and a factor of safety against liquefaction. Although these are simple and convenient to use, they are based on laboratory test results on specific sands like Fuji River sand in the method by Ishihara and Yoshimine (1992) and Zhang et al. (2002). So, their application on sands with variations in grading and mineralogy may result in inaccurate predictions. Additionally, studies like Cubrinovski et al. (2018) emphasized the importance of effective stress analysis to comprehensively understand the response of soil deposits. Since there is a dynamic interaction between layers during liquefaction, relying solely on empirical charts may yield an oversimplified solution.

A better understanding of deformation behavior and its magnitude before and after liquefaction is necessary. The settlement during the shaking is relatively small compared to the one that develops right after the earthquake has ended (i.e., post-liquefaction settlement; Lambe and Whitman 1985). Thus, the post-liquefaction settlement is a critical aspect of geotechnical engineering that requires careful consideration in earthquake-prone regions.

2.2 Post-liquefaction

In addition to the liquefaction triggering analysis, a reconsolidation analysis or post-liquefaction settlement study is crucial to assess the potential damages to man-made structures (Ishihara et al. 2016). Field observations of seismic-induced settlements in saturated sands range from zero to 20 inches (Tokimatsu and Seed 1987). Numerous case histories, centrifuge tests, empirical models, and numerical analyses have been conducted to predict reconsolidation settlement. For instance, Wu and Seed (2004) proposed an empirical procedure for estimating seismically induced ground settlement in nearly level ground based on post-liquefaction reconsolidation volumetric strain correlations. The exploration of post-liquefaction settlement is still a relatively less established field, leaving ample room for further advancements in the development and validation of engineering tools and methods (Seed et al. 2003). The primary objective of reconsolidation analysis is to predict soil surface settlement, which is vital for evaluating the response of structures.

2.2 POST-LIQUEFACTION

Different studies have described the post-liquefaction reconsolidation behavior of liquefied sands. The Terzaghi consolidation theory is widely used to study consolidation-related problems in geotechnical engineering (Terzaghi 1965). The consolidation equation by Terzaghi involves mass balance, Darcy's law, and the effective stress principle. The equation assumes (a) constant saturation of the soil, coefficients of hydraulic conductivity, and one-dimensional stiffness, (b) incompressibility of both soil grains and pore fluid, and (c) alterations in porosity can be associated with the changes in effective stress. However, Terzaghi's consolidation theory does not perform well in post-liquefaction reconsolidation, as the parameters such as the coefficient of consolidation (c_v), which in turn depends on soil stiffness and permeability, cannot be assumed constant as in the original theory during reconsolidation. Key observations from different centrifuge tests have revealed that the value of c_v at the beginning of reconsolidation should be considerably smaller than that at the end (Zeybek and Madabhushi 2023). As sand approaches a state of near-zero effective stress, there is an increase in permeability and the one-dimensional stiffness drops. Capturing the evolution of these material parameters during post-liquefaction is essential to better understand settlement and time-rate predictive tools.

In addition, several theories have been proposed to describe the progression of the liquefaction and reconsolidation mechanisms within one layer. Florin (1961) proposed the solidification front theory for reconsolidation based on 1-g shaking table tests. Their findings indicated that liquefaction initiates from the surface and progresses downward, with excess pore pressures dissipating from the base to form a solidified sand layer. Scott (1986) modified this theory by integrating it with Terzaghi's consolidation theory, finding additional excess pore pressures that gradually dissipate and contribute to the layer's settlement. Kim et al. (2009) showed that the solidification front velocity does not remain constant; instead, it decreases as it moves toward the surface. There are various issues regarding these existing studies related to solidification theory. First, the advancement of the solidification front is determined by empirical approaches, which are challenging to generalize for different sand types (Brennan and Madabhushi 2011). Second, the properties associated with the solidified soil are not realistic. Thirdly, it has been observed that the values of hydraulic conductivity higher than the expected values are required to match the experimental data.

Researchers have also attempted to estimate soil parameters by back-analyzing experimental data (Zhang et al. 2010). One such attempt used a Fourier series solution of Terzaghi's differential equation for consolidation during reconsolidation and back-calculated values of the

coefficient of consolidation (c_v) from excess pore pressure dissipation data (Brennan and Madabhushi 2011). Another attempt proposed a simplified exponential equation to quantify the rates of excess pore pressure dissipation. Both methods showed a satisfactory fit to experimental data. However, a significant challenge persists in determining the deformation of the soil matrix and its interaction with pore pressures (Goren et al. 2010). Such attempts to predict reconsolidation provide a technique to explore liquefied soil without the additional complexity of dynamic loading, but there is still much uncertainty about the fundamental mechanism.

Adamidis and Madabhushi (2016) proposed an effective stress-dependent differential equation to predict the reconsolidation of a sand deposit without separating the layer into distinct segments: upper liquefied and lower solidified parts. They considered all the assumptions of Terzaghi's original consolidation theory except for the one requiring constant coefficients of 1-D stiffness and hydraulic conductivity. The proposed algorithm effectively replicated the observed reconsolidation process in two geotechnical centrifuge tests. Their major conclusion was that the variation of 1-D stiffness has a major role in reconsolidation. The traditional consolidation analyses fall short of capturing reconsolidation due to the assumption of linear elasticity. Although a change in the coefficient of hydraulic conductivity impacts the reconsolidation process, its contribution is more important on the time rate of settlement, and it is comparatively less significant in terms of settlement magnitude. However, the proposed equation by Adamidis and Madabhushi (2016) cannot be applied in connection with dynamic loading scenarios, where volume compaction occurs primarily due to shearing.

The field case histories for post-liquefaction settlement of granular soils are significantly smaller and possess larger uncertainties than those for liquefaction triggering (NASEM (National Academies of Sciences and Medicine) 2016). Researchers have expanded, reinterpreted, and filtered case histories based on deformation patterns, while also applying quality assessment ratings to residual shear strength (Idriss and Boulanger 2007; Kramer and Wang 2015; Olson and Stark 2002; Seed and Harder Jr 1990; Stark and Mesri 1992). There are three general types of approaches to estimating large seismic-induced liquefaction settlements: (1) statistically derived empirical methods, (2) simple static limit equilibrium analyses incorporated with engineering judgment, and (3) fully nonlinear mesh-based (i.e., finite element or finite difference) numerical analyses (Seed et al. 2003). The empirical methods are based on case histories and back-analyses of previous databases and involve probabilistic or statistically derived equations for estimating final total displacements. Although there are

empirical relationships for predicting residual strength (critical parameter for seismic stability analyses) and deformation after shaking ceases, these are constrained by the limited parameter ranges of the case histories from which relationships are derived. The second approach is estimating potential substantial liquefaction-induced displacements based on evaluating deformations required to re-establish static equilibrium. This needs meticulous evaluation of the critical mode of failure or deformation.

The final approach is numerical modeling, in which finite element and finite difference analyses are the most widely used and complex approaches. In the past, these methods were principally employed for relatively critical studies, but now these methods are widely used for analyzing soil deformations (Seed et al. 2001). Settlement resulting from reconsolidation after liquefaction is caused by the volumetric strains that emerge across the underlying soil profile, and it is still a challenge to numerically model this phenomenon (Byrne et al. 2004). Additionally, 2D numerical models cannot replicate the multi-directional seismic motion, which may yield an underprediction of post-liquefaction settlement (Gingery 2019). The primary challenge with these approaches is the difficulty of finding material constitutive models (i.e., stress-strain relationships). Conventional constitutive models do not adequately represent post-liquefaction volumetric strains due to sedimentation under zero effective stress (Boulanger and Ziotopoulou 2015). These models do not capture the decrease in stiffness during post-liquefaction reconsolidation, and consequently, they tend to highly underestimate the one-dimensional settlements triggered by liquefaction. In this regard, few constitutive models have been developed to account for the post-liquefaction reconsolidation strains; some of these are described in section 2.5.

2.3 Liquefaction Assessment

Over the years, significant progress has been confined to improving the assessment of the likelihood of liquefaction triggering in clean, sandy soils. Earthquakes have provided numerous data and lessons, highlighting challenges related to silty and gravelly soils, as well as post-liquefaction deformation issues (Green et al. 2014). The schematic diagram showing the steps towards engineering treatment of soil liquefaction is illustrated in Figure 1. The first step involves (1) assessment of liquefaction potential. Once the occurrence of liquefaction is determined, the following step is to assess the consequences of liquefaction potential. So, the second step is (2) analyzing existing post-liquefaction strength and resulting post-liquefaction

stability. If there is insufficient post-liquefaction stability, then the third step is (3) evaluating the post-liquefaction deformation/displacements. It is also important to (4) estimate the impact of deformations induced by liquefaction on the performance of structures and other engineering facilities. Ultimately, if the criteria for acceptable performance are not well-defined, the next step is to (5) implement and evaluate necessary engineering mitigation measures (Seed et al. 2003). There are many ongoing evolutions of new methods for mitigation of liquefaction hazards, such as improving soil properties by using compaction and grouting, drainage and dewatering, soil replacement techniques, compaction piles and stone columns, dynamic compaction, soil improvement techniques (mixing cement, lime, or other stabilizing agents), geosynthetic reinforcement, seismic retrofitting, and so on (Nicholson 2014).

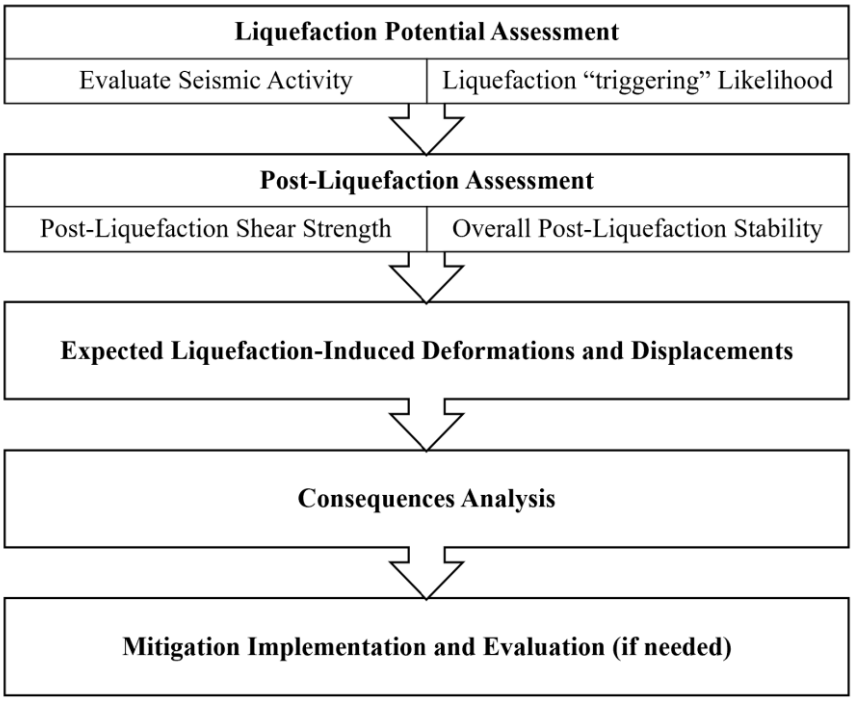

Figure 1. Key Elements of Liquefaction Assessment (Seed et al. 2003).

2.4 Stone Columns as a Mitigation Measure

Among various remediation measures, using stone columns is a quite recent technique compared to other soil densification methods (Green et al. 2008). A stone column is a vertical cylindrical structure in the ground of densely compacted stones or gravel. Typically, these columns have cross-sectional diameters ranging from 75cm to 150 cm, which is extended to reach bedrock or hard layers, but there are instances where floating columns are also installed (Poorooshasb and Meyerhof 1997). The stone columns can be installed by two methods,

depending on the soil condition of the site: Vibro-displacement and Vibro-replacement. Vibro-displacement is a technique wherein the vibro-probe penetrates through vibration and with the assistance of compressed air to achieve the necessary depth. The stone column is then installed by introducing gravel through a distinct gravel duct located alongside the vibro-probe. Vibro-replacement is a technique in which the in-situ soil is replaced with granular materials such as compacted stones and gravel, particularly when the design density cannot be attained through vibrations alone. Vibro displacement proves to be more suitable than many other soil improvement methods for mitigating liquefaction (McCabe et al. 2009).

In the case of soil reinforced with stone columns, if high excess pore pressure is generated within the enhanced soil mass, the resulting shear stresses during an earthquake can be distributed between the stone columns and the adjacent soil mass (Kirsch 2010). This distribution of shear stress depends on the comparative stiffness of composite materials, enhancing the overall stability of the system (Bhochhibhoya et al. 2023). The efficacy of stone columns has been observed in past earthquakes. For instance, the case study of the Dean Stand at Lancaster Park during the Christchurch earthquake supplied valuable insights concerning the performance of stone columns. The study showed that the overall design performance of stone columns was achieved, but they sustained substantial damage and were unreliable for future catastrophic events (Green et al. 2011). Nevertheless, the case study summed up the fact that ground improvement measures like stone columns are advantageous to withstand higher levels of earthquake shaking (Alexander et al. 2019).

Adalier et al. (2003) demonstrated that stone columns are an effective countermeasure in the remediation of liquefaction-induced settlement using a series of four centrifuge model tests, first without stone columns and then others with stone columns, both under free-field conditions and with a surcharge of foundation load. They focused on exploring the site stiffening effects after the placement of stone columns. Asgari et al. (2013) and Badanagki et al. (2018) validated the drainage effects on reducing settlement in the free field conditions using numerical analysis as well as centrifuge tests. Asgari et al. (2013) presented the 3D numerical analysis of several parameters (stone column diameter, permeability, ground motion characteristics, and their interactions) and their effects on liquefaction, lateral spreading, and shear-strain of the behavior of sand subjected to different seismic events. They used the constitutive model in OpenSees based on the multi-surface-plasticity theory for frictional cohesionless soils proposed by Prevost (1985). The model was proposed to simulate the

liquefaction-induced shear strain accumulation mechanism in sands, but reconsolidation settlement was not evaluated (Elgamal et al. 2003).

Reconsolidation analysis can provide valuable insights regarding liquefied soil, but there still exists a gap in understanding the process, regarding the increased settlement rate of liquefied soil during shaking compared with that of reconsolidation (Adamidis and Madabhushi 2016). Gingery (2019) is among the limited studies that examined the axial reinforcing effects of stone columns using a numerical approach and developed a constitutive model (modified Mohr-Coulomb model) to represent post-liquefaction reconsolidation behavior without accounting for soil responses during an earthquake. In this regard, more comprehensive investigations are required to thoroughly assess the efficacy of stone columns in mitigating post-liquefaction settlement.

2.5 Constitutive Modeling

2.5.1 General Observations

A constitutive model is used to model the stress-strain behavior of soil via a numerical formulation. Constitutive models are generally calibrated using laboratory tests. There has been a significant development in the field of soil constitutive models for sands over the past few decades (Andrianopoulos et al. 2010; Prevost 1985; Taiebat and Dafalias 2008; Ziotopoulou and Montgomery 2017). Different constitutive models may have advantages and limitations based on their use and applicability. For example, linear elastic models and elastic perfectly-plastic models have been commonly used for non-liquefiable layers, while total stress models (e.g., Beaty model; Beaty 2001), loosely-coupled effective stress models (e.g., Finn model; Finn et al. 1976), and fully-coupled effective stress models (e.g., PM4Sand; Ziotopoulou and Boulanger 2013) are generally used for liquefiable layers. There are numerous constitutive models available to simulate liquefaction triggering and cyclic loading deformations, such as WANG2D (Wang et al. 1990), PDMY02 (Elgamal et al. 2003), UBCSand (Beaty and Byrne 2011), PM4Sand (Ziotopoulou and Boulanger 2013), and SANISAND (Yang et al. 2022), among others.

The choice of constitutive model depends on the need to model certain aspects of material behavior. These may include stress and strain relationships, generation of excess pore pressure, and strain softening (Ziotopoulou and Boulanger 2013). For modeling soil liquefaction, it is

essential to replicate stress-strain relations, pore pressure development, and dissipation, both in monotonic and cyclic loading conditions. Furthermore, soil models designed for liquefaction analysis should accurately represent the behavior described by empirical relations for liquefaction triggering and post-liquefaction responses.

Settlement due to post-liquefaction reconsolidation results from volumetric strains developed within the soil profile. It is challenging to model these volumetric strains numerically as the conventional approach of separating the strains into elastic and plastic components cannot accurately reflect the post-liquefaction volumetric strains caused by sedimentation under negligible effective stress (Boulanger and Ziotopoulou 2015). It is essential to effectively simulate the redistribution of pore pressure following shaking to estimate post-liquefaction volumetric strains accurately. Simple, realistic, and computationally efficient cyclic constitutive models are ideally required to solve boundary-value problems related to large post-liquefaction deformation.

Furthermore, constitutive models capable of capturing post-liquefaction response can be categorized into two types: (a) simpler models that particularly focus on post-liquefaction settlement (e.g., Modified-Mohr Coulomb; Gingery 2019) and (b) advanced models developed to account for liquefaction triggering that have been extended to incorporate post-liquefaction response (e.g., PM4Sand; Ziotopoulou and Montgomery 2017). In general, these models account for reconsolidation behavior by reducing stiffness. This reduction in stiffness is governed by various factors depending on the model, such as fabric parameters, plastic strain, or pore pressure ratio. A detailed description of a selection of such constitutive models is presented in sections 2.5.2 and 2.5.3.

2.5.2 Constitutive Model for Post-Liquefaction Settlement

To model the post-liquefaction reconsolidation behavior of sand, a basic constitutive model was developed and implemented in FLAC by Gingery (2019). The main purpose of this model is to capture the behavior involved in reconsolidation. The model was developed to achieve the following objectives: (a) to produce a target volumetric strain in a free field condition, (b) to represent the weakened and softened state of the liquefied soil and the gradual re-stiffening and strengthening that happens during porewater pressure dissipation and reconsolidation. Considering these, an effective stress-based model was developed that varied the constrained modulus (M) with effective stress and excess pore pressure ratio:

$$M = M_{liq} + (M_0 - M_{liq}).\left[\frac{\sigma'_{m,liq} - (1 - r_{u,max})\sigma'_{m0}}{r_{u,max}.\sigma'_{m0}}\right]^n \quad (1)$$

where σ'_{m0} is the initial mean effective stress whereas, $\sigma'_{m,liq}$ is the mean effective stress during the reconsolidation process. M_0 and M_{liq} are pre-liquefaction and liquefied constrained modulus, respectively. $r_{u,max}$ is the maximum excess porewater pressure ratio during liquefaction and n is an exponent used as a calibration constant. Although the value of $r_{u,max}$ obtained in the centrifuge model was 1.0 for liquefied soil, Gingery (2019) used $r_{u,max} = 0.96$ to prevent potential numerical instability problems related to a condition of zero effective stress.

During liquefaction and reconsolidation phenomena, the shear modulus (G) and bulk modulus (K) are updated based on their relationship with the constrained modulus (M) and Poisson's ratio (ν) using the following equations:

$$\mathrm{G} = \frac{M(1 - 2\nu)}{2(1 - \nu)} \quad (2)$$

$$\mathrm{K} = \frac{M(1 + \nu)}{3(1 - \nu)} \quad (3)$$

In short, the post-liquefaction reconsolidation strains are computed by using an integral under a 1-D framework:

$$\varepsilon_{vol} = \int_{\sigma'_{v0}}^{\sigma'_{v,liq}} \frac{1}{M}\, d\sigma'_v \quad (4)$$

where $\sigma'_{v,liq} = \left(1 - r_{u,max}\right)\sigma'_{v0}$. σ'_{v0} is the initial vertical effective stress. $\sigma'_{v,liq}$ is the effective stress during liquefaction and reconsolidation.

One of the major drawbacks of this model is that it does not consider the settlement of structures or footings due to shear-related effects, nor settlement caused by ejecta. Additionally, this model cannot quantify the soil response during shaking.

2.5.3 Constitutive Models for Liquefaction Triggering and Post-Liquefaction Behavior

These are typically the extension of models previously developed for liquefaction triggering. In these models, the post-liquefaction behavior of sands is included in terms of a stiffness degradation rule without modifying hydraulic conductivity (k). The extended versions of these models are equipped with a switch or a curve-fitting factor that controls the degree of stiffness reduction. Two examples of such models are UBC3D-PLM and PM4Sand.

2.5.3.1 UBC3D-PLM

UBCSand is an elastoplastic effective stress model developed on the formulation of hyperbolic relation between stress ratio and plastic shear strain. The model is fully coupled, and the behavior of the solid skeleton is represented by the effect of pore fluid introduced through volumetric stiffness. Beaty and Byrne (1998) presented the early extension of UBCSand subjected to earthquake loading. Over the years, this model has been modified to better calibrate complex seismic loading. The UBC3D-PLM model, derived from the UBCSand model by Puebla et al. (1997) and Beaty and Byrne (2011), is also an effective stress model. The major distinction between the UBCSand and its extended version is that the latter is generalized in 3-D formulation (Petalas and Galavi 2013). The UBC3D-PLM model employs the Mohr-Coulomb yield criterion within a three-dimensional space defined by principal stresses. Furthermore, it integrates a revised non-associated plastic potential function originating from the Drucker-Prager criterion to preserve the assumption of stress-strain alignment in the deviatoric plane for a stress path starting from the isotropic line (Diaz-Segura 2015).

While modeling the cyclic liquefaction of sands, numeric volumetric locking is given an essential consideration in UBC3D-PLM. When the stress path intersects the yield surface determined by the peak friction angle, the constant evolution of volumetric strains occurs as a result of the formulation of the flow rule (Petalas and Galavi 2013). Because of this, the original UBCSand model is not able to simulate the change in soil stiffness resulting from reconsolidation in loose sandy soils or the cyclic mobility of dense cohesionless soils, as observed in experimental studies (Ju and Vassalos 2015). This issue is resolved in the formulation of UBC3D-PLM sand by reducing the plastic shear modulus from the primary value $\left(K_{G,primary}^{p}\right)$ to a reduced one $\left(K_{G}^{p}\right)$ according to the following equation:

$$K_G^p = K_{G,primary}^p * E_{dil} \tag{5}$$

where E_{dil} is a factor that controls the degradation which is formulated as shown below:

$$E_{dil} = max\left(e^{-110\varepsilon_{dil}}, fac_{post}\right) \tag{6}$$

where ε_{dil} is the accumulation of plastic deviatoric strain generated during the soil element dilation, $fac_{post}$is the post-liquefaction factor.

The parameter fac_{post} is obtained from calibration and curve fitting and typically ranges between 0.2 and 1. fac_{post} must be very low in order to attain a pore pressure ratio (r_u) of 1 i.e., to cause liquefaction triggering . Otherwise, even when a minimum shear modulus value is reached, subsequent loading cycles will be unable to induce any additional increases in pore pressures. Because of this, the soil will never attain the full liquefaction state. Moreover, this factor controls the plastic behavior of soil at the end of the reconsolidation stage.

Studies like Arboleda-Monsalve et al. (2017) and Makra (2013) have shown that although UBC3D-PLM can simulate the development of excess pore pressure during cyclic loading, the post-liquefaction behavior in terms of reconsolidation settlement cannot be predicted because the model cannot simulate the re-sedimentation process of soil in the post-liquefaction stage.

This model exhibits several additional limitations. Firstly, the model requires the calibration of 13 parameters for numerical simulation, which is not pragmatic for industrial purposes. It lacks compaction hardening and the representation of cyclic loading and the representation of liquefaction behavior does not always align with reality. Moreover, there tends to be an overestimation of damping in dynamic calculations.

2.5.3.2 PM4Sand Model

The PM4Sand model adheres to the fundamental principles of the stress-ratio controlled, critical-state compatible, bounding-surface plasticity models for sands. This two-dimensional constitutive model follows the original concept of Dafalias and Manzari (2004), which is predicated on bounding surface plasticity and critical state framework outlined by Schofield and Wroth (1968) and Wood (1990). This model is specifically developed for plane-strain conditions by considering in-plane stresses (Chen 2020). The soil model is founded on effective stresses and accounts for the generation of excess pore pressure induced by cyclic or dynamic loading in undrained conditions.

The PM4Sand model by Boulanger and Ziotopoulou (2013) accounts for increments in both plastic and elastic strains. These increments comprise volumetric and deviatoric terms. Elastic strain increments are generated by the prevailing stress levels, constrained by the soil material's shear modulus (G) and bulk modulus (K) (Chen 2020). On the other hand, plastic strain increments are induced by the loading index (L) and are limited by the dilatancy (D) and distance between stress levels relative to the position of the yield surface, as determined by the normal tensor (n) (Toloza 2018). As a result, excess pore pressure is generated under undrained conditions, and it is computed through the reduction of effective stresses in the soil caused by volumetric strain increments (Quevedo 2019). Boulanger and Ziotopolou (2013) have presented comprehensive explanations of all PM4Sand constitutive equations and terminologies as well as simulated the element responses over a wide range of conditions. The PM4Sand includes the traditional additive decomposition of strains; hence, it is unable to account for reconsolidation settlements naturally. Generally, such stress-ratio-based models represent reconsolidation as an elastic process, yielding only minor volumetric strains and underestimating the total post-liquefaction settlements.

Within the PM4Sand model framework, 13 parameters can be determined by the user. These can be categorized into two groups; these are (a) primary parameters: D_{R0}, G_0, h_{p0}, and p_A (most significant parameters for model calibration) and (b) secondary parameters: these include $e_{max}, e_{min}, n^d, n^b, \phi_{cv}, \nu, Q, R,$ and $PostShake$ (these have default or recommended values, but they can also be modified based on different conditions). The parameters of the PM4Sand model with their notations and names are summarized in Table 1.

Table 1. PM4Sand parameters used in Plaxis 2D based on Boulanger and Ziotopoulou (2017).

Parameters	Notation	Default Values
Relative Density	D_r	Calibrated
Shear Modulus coefficient	G_0	Calibrated
Contraction Rate Parameter	h_{p0}	Calibrated
Atmospheric pressure	p_A	101.3 kPa
Maximum void ratio	e_{max}	0.8
Minimum void ratio	e_{min}	0.5
Bounding surface parameter	n^b	0.5
Dilatancy surface parameter	n^d	0.1
Constant volume friction angle	ϕ'_{cv}	33^0
Poisson's ratio	ν	0.3
Critical state line parameter	Q	10
Critical state line parameter	R	1.5
Post-liquefaction factor	PostShake	1 or 0

Boulanger and Ziotopolou (2017) extended the pre-existing PM4Sand by introducing an approximate approach to consider sedimentation strains during reconsolidation. This method has been incorporated into the model to provide more accurate estimates of reconsolidation strains by reducing post-earthquake elastic shear and bulk moduli. The reduced elastic moduli increase the post-liquefaction reconsolidation strains, compensating for sedimentation strains that are not explicitly accounted for in the model. Users have the choice to activate this factor after the end of a strong shaking by just a simple switch (no additional material parameter is required); hence, the reconsolidation strains are evaluated in the remaining part of the simulation.

The reduction in elastic shear and bulk moduli depends on the maximum fabric parameter (z_{max}) (a model input), the cumulative fabric parameter (z_{cum}) (a damage measure), the current stress ratio (M_{cur}), and the slope of the dilatancy line (M_d). Additionally, sedimentation mean effective stress (p'_{sed}) is defined to control the range of mean effective stresses (p') over which reconsolidation strains are intensified, i.e., elastic moduli are degraded, as given by:

$$p'_{sed} = p'_{sedo} \left(\frac{z_{cum}}{z_{cum} + z_{max}}\right) . \langle 1 - \frac{M_{cur}}{M_d} \rangle^{0.25} \tag{7}$$

If $\langle 1 - \frac{M_{cur}}{M_d} \rangle^{0.25}$ is negative, the MacCauley brackets return 0. The sedimentation coefficient p'_{sedo} was calibrated as $20kPa$. Likewise, the elastic moduli reduction factor F_{sed} is evaluated as a function p'_{sed} and p'as,

$$F_{sed} = F_{sed,min} + \left(1 - F_{sed,min}\right).\left(\frac{p'}{20.p'_{sed}}\right)^2 \leq 1 \tag{8}$$

where $F_{sed,min}$ is the smallest possible value that F_{sed} can reach. The value of F_{sed} gradually decreases from unity towards $F_{sed,min}$ as z_{cum} continuously increases when M_{cur} is less than M_d. The formulation of the parameter $F_{sed,min}$ based on the relative density (D_r) according to the empirical correlation proposed by Ishihara and Yoshimine (1992) is given by:

$$F_{sed,min} = 0.03\, exp(2.6\, D_r) \tag{9}$$

During the modeling phase of post-liquefaction reconsolidation, the elastic shear (G) and bulk (K) moduli assigned to the soil are computed by multiplying the reduction factor (F_{sed}) with the corresponding elastic moduli of the soil, calculated using the original constitutive relationships:

$$G_{post-shaking} = F_{sed}.G \tag{10}$$

$$K_{post-shaking} = F_{sed}.K \tag{11}$$

In summary, in the PM4Sand model, the reconsolidation behavior should only be incorporated after the end of strong shaking. A limitation of the extended PM4Sand model is that it does not implicitly account for a change in hydraulic conductivity (k) during reconsolidation; hence, it is expected that the rate of settlement predicted, and excess pore pressure dissipation will be underpredicted, although the final magnitude will remain the same for both constant and variable k, as presented by (Basu et al. 2022).

Chapter 3

Materials and Methodology

The objectives of this study are to scrutinize the reconsolidation settlements of a liquefiable soil deposit subjected to various levels of shaking intensity and estimate the efficacy of stone columns in mitigating reconsolidation settlement. To accomplish such goals, the following methodology is proposed.

First, the PM4Sand model is selected to account for cyclic response and reconsolidation settlements before and after installing stone columns. The analysis is performed in plane strain conditions using the finite element method, Plaxis 2D. Plaxis is a geotechnical finite element software that specializes in simulating soil-structure interaction, including liquefaction. There are few advanced constitutive models available in the software platform, particularly for simulating liquefaction. Among them, the PM4Sand model successfully captures the dynamic behavior of sands subjected to various loading conditions, including pore pressure generation, liquefaction, and reconsolidation (Armstrong et al. 2013; Boulanger et al. 2018; Kamai and Boulanger 2013). This is a highly appealing constitutive model for practical applications because of a small number of parameters to be calibrated, i.e., apparent relative density D_{R0}, the shear modulus coefficient G_0, and the contraction rate parameter h_{po}.

In any finite element analysis, regardless of whether a basic or advanced constitutive model is employed, the initial step involves determining the model parameters for the specific soil type and loading circumstances. For liquefaction constitutive models, this can be a complex process, as they often involve parameters that cannot be directly derived from lab tests (Makra 2013). Since most of these constitutive models are stress-path dependent and are highly complex, it is necessary to calibrate these parameters before practical implementation in a project. It is imperative for the accuracy of the analysis to determine parameters through appropriate lab tests that align well with the field's existing loading conditions.

In this study, validation of the potential for the PM4Sand model in quantifying liquefaction triggering and post-liquefaction settlement has been carried out by replicating the experiment on Ottawa F-55 sand developed by Thevanayagam et al. (2009). The material properties used

were based on the calibrated lab data for the same sand reported by Basu et al. (2022). They performed the analysis utilizing FLAC which is an explicit finite difference code. The results obtained from Plaxis 2D were compared with the experimental observations and also with those reported by Basu et al. (2022).

After validation of the numerical framework, a new numerical model has been proposed to investigate the post-liquefaction behavior before and after installing stone columns. Furthermore, a detailed parametric analysis under different ground motion intensities was performed along with a comparison of reconsolidation settlement was done with and without the extension of modulus reduction in PM4Sand. Finally, the post-liquefaction settlement was evaluated by analyzing the numerical model with a footing load. The details of this analysis are presented in Chapter 4.

3.1 Validation of Numerical Framework

The effectiveness of the numerical approach must be verified before performing a detailed numerical study. To accomplish this, the validation exercise includes developing a numerical model based on a physical shaking experiment performed on non-reinforced ground and then comparing the numerical results with the experimental findings (Thevanayagam et al. 2009) and previous numerical studies (Basu et al. 2022).

3.1.1. Experimental Study on Ottawa F-55 sand (Thevanayagam et al. 2009)

Thevanayagam et al. (2009) developed a 1-g laminar box shaking system. They conducted two shake tests: (a) the first test on level ground, referred to as LG-0, and (b) the second test on gently sloping ground, denoted as SG-1. In the present study, the test with the level ground (LG-0) has been considered. The soil depth in LG-0 was 5m, as shown in Figure 2. The groundwater table was placed at the top of the soil surface for the model. Relative density profiles were acquired using data from bucket density tests and relative density correlations based on cone penetration resistance (Jamiolkowski et al. 2003; Schmertmann 1976). The soil profiles obtained from field density tests and static CPT tests were consistent, and they indicated an average relative density of $D_{R0} = 40\%$ and a normalized cone penetration resistance of $q_{c_1N} = 50$. Normalized shear wave velocity of around V_{S_1} = 115 m/s was obtained from the system identification techniques using soil response subjected to sinusoidal cycles

(Dobry et al. 2011). Based on these values, they concluded that the soil deposit of Ottawa F-55 sand represented loose, liquefiable, young sand deposits.

The harmonic input waves at a frequency of 2 Hz were used in the experiment in four phases. The first ten cycles consisted of a 0.01g amplitude shaking applied as non-destructive shaking. The succeeding motion consisted of subsets of motions, each of 10 seconds duration with amplitudes of 0.05g, 0.15g, and 0.3g, respectively. Figure 3 presents the acceleration time history applied at the base of the model. This experiment was chosen in this study because it provided ample data to characterize both the evolution of excess pore pressures during and after liquefaction. Additionally, the original authors did not outline any problems with settlement measurements that might have affected the validity of the comparisons.

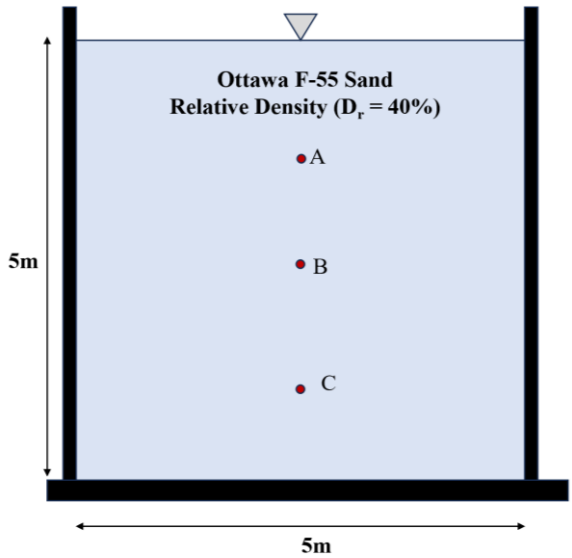

Figure 2. Schematic diagram of the experiment conducted by Thevanayagam et al. (2009) with the location of pore pressure transducers and settlement sensor.

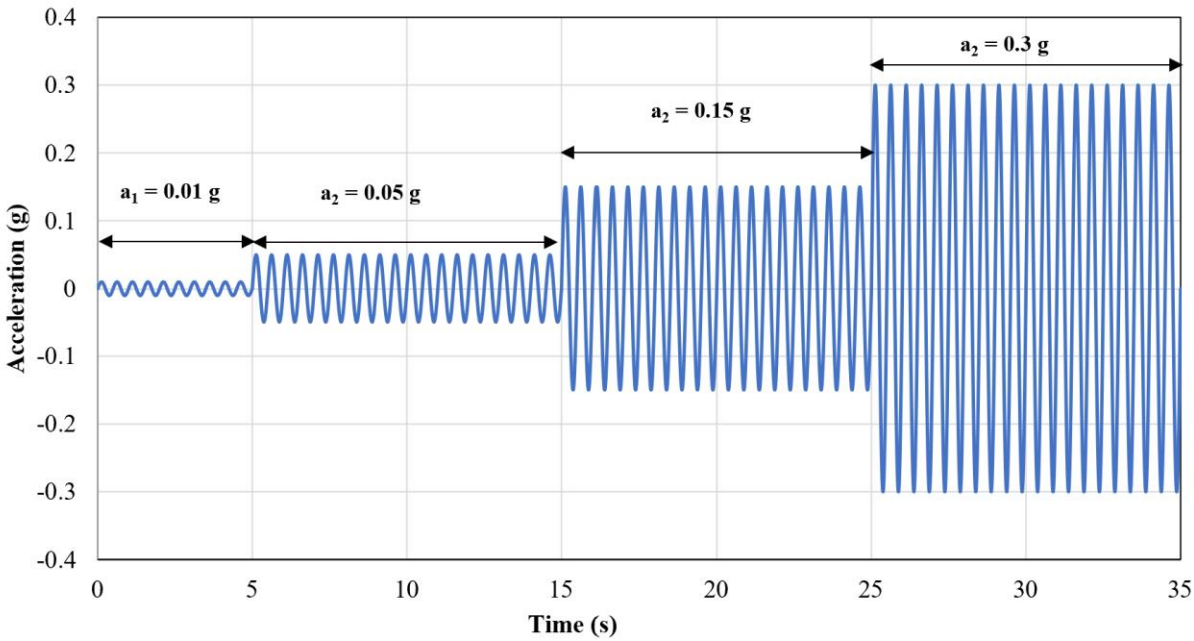

Figure 3. Input ground motion used in the experiment by Thevanayagam et al. (2009).

3.1.2 Previous Numerical Study (Basu et al. 2022)

In addition to the experimental data, this study also considers the numerical results obtained by Basu et al. (2022) to validate the numerical framework. They modeled three centrifuge tests (Adamidis and Madabhushi 2016; Mehrzad et al. 2018; Ramirez et al. 2018) and two shake table tests (Ecemis (2021); Thevanayagam (2009)) emphasizing settlement of liquefied soil under free-field conditions. They performed their models using FLAC version 8.0.

The simulation of Thevanaygam et al. (2009) shake table test was conducted without applying any scaling. For their study, they utilized the PM4Sand constitutive model for computational efficiency and applied 1D columns corresponding to a soil column at the centerline of the experimental model. Results were compared with instrument readings in the vicinity of the center of the model. The simulations were conducted in three stages: static equilibrium, dynamic phase, and post-liquefaction phase, with applied hydraulic and mechanical boundary conditions. For the hydraulic boundary conditions, free drainage was allowed from the top boundary of the model whereas no flow was allowed from the sides and the bottom boundary of the model. For the mechanical boundary conditions, horizontal movements were normally fixed at the sides, whereas the horizontal and vertical movements were fixed at the bottom (fully fixed). During the dynamic phase analysis, input motions were applied in the form of acceleration-time histories along the base of the model in which the periodic boundary conditions were implemented along the sides, with a rigid base at the bottom of the model.

Rayleigh damping of 0.5% was implemented to reduce numerical noise. The modelers used a scaling factor for permeability in the reconsolidation phase to speed up the process. For the reconsolidation phase, to increase the rate of dissipation of excess pore pressure, they reduced the calculation time by increasing the permeability in all zones by approximately 25 folds.

Since there was insufficient laboratory data to develop liquefaction-triggering curves, Basu et al. (2022) chose the h_{po} values for these sands in such a way that they matched the results of developed excess pore pressure during the dynamic phase, contraction cycles, dilation, and residual excess pore pressure at the end of shaking recordings of the experiment. The default values were assigned to the secondary PM4Sand parameters except for n_b to match the strain rate accumulation that developed after liquefaction triggering, as explained by Basu et al. (2022). Table 2 presents the calibration parameters used for Ottawa F-55 sand. Based on these parameters, they examined the significance of calibrating post-liquefaction stiffness and hydraulic conductivity to accurately capture the generation of the excess pore pressure and reconsolidation settlement. However, despite the variation in hydraulic conductivity, their rates of dissipation significantly varied from the experiment.

Table 2. Geotechnical properties of the Ottawa F-55 sands.

Sand	D_{R0} (%)	G_S	e_{max}	e_{min}	k (cm/s)	h_{po}	ϕ'_{crit}	n_b	G_0
Ottawa F-55	40	2.65	0.8	0.61	0.012	0.12	33o	0.5	192

3.1.3 Plaxis 2D Model (Present Study)

In this study, Ottawa F-55 sand was modeled using the implicit finite element program Plaxis 2D. A plane strain numerical model with a geometry of 5mx5m in length and thickness was simulated without scaling. The model analyzed for validation purposes is shown in Figure 4. The whole geometry of the FEM model domain was discretized using 15-node triangular elements. The optimization of mesh size was done considering both solution time for each analysis as well as the accuracy of the results. Hence, the mesh size was considered to be fine as shown in Figure 4. The PM4Sand constitutive model was used for both the dynamic and consolidation stages of analysis.

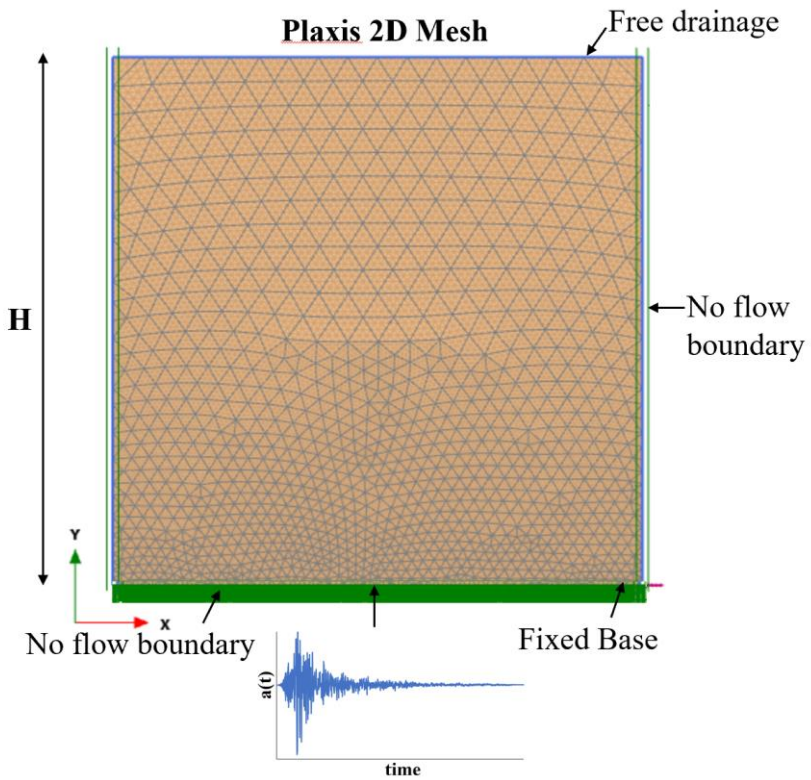

Figure 4. Plaxis 2D mesh for plane strain model highlighting their boundary conditions.

Simulations were performed in three stages: (a) static equilibrium (Phase I), (b) dynamic phase (Phase II), and (c) reconsolidation phase (Phase III), as shown in Table 3. In the first stage, Phase I, the initial stress state of the soil was generated using the gravity loading option. It was selected to ensure stress field equilibrium at the end of the initial phase. Hydrostatic pore pressure conditions were generated throughout the model corresponding to the depth of the groundwater table as per the experiment. The PM4Sand model has less accuracy in simulating such static loading conditions because the model was developed and calibrated for dynamic loading conditions; hence, it has been recommended to use an equivalent model instead of PM4Sand material to achieve the static equilibrium conditions (Plaxis 2018). In this study, the static equilibrium was established using a linear model equivalent to PM4Sand.

In all three stages, the flow boundary conditions (hydraulic boundary) permitted free drainage from the top boundary of the model, whereas the sides and the bottom boundary conditions were closed (no flow boundaries). Deformation boundary conditions varied during the analysis. The details of boundary conditions are presented in Table 3. In the first phase, during static equilibrium, boundaries at sides (along the X-axis) were normally fixed, such that horizontal

movement was fixed, but vertical movement was allowed. The top boundary was free, but the bottom boundary was fixed at the base without allowing vertical or horizontal movement.

To estimate the reconsolidation response of PM4Sand, it has been recommended to divide the analysis into two calculation stages: (i) the dynamic phase in which the strong motion with appropriate dynamic time interval is considered and (i) the reconsolidation phase considering the remaining dynamic time interval. The dynamic time interval refers to the overall time period considered in the corresponding phase of dynamic calculations. The original input motion (Figure 3) with the duration of 35 seconds used in the experiment by Thevanayagam et al. (2009) was modified in the present study by adding a weak motion as shown in Figure 5.

The second stage (Phase II) was simulated using the "Dynamic with Consolidation" calculation type in Plaxis2D. A strong input motion with a dynamic time interval of 35 seconds was applied along the model's base. The rate of excess pore pressure generation surpasses the rate of dissipation during intense shaking, so there is a net accumulation of excess pore pressure (Ishihara and Yoshimine 1992). Hence, to account for the dissipation of excess pore pressure that may occur during shaking, the calculation type, "Dynamic with consolidation," was selected for the dynamic phase to allow dynamic generation and subsequent dissipation of excess pore pressures within the short time of the application of the dynamic loading. In this stage, the material was changed to PM4Sand such that the model's internal variables were initialized in accordance with the stress state of the static phase prior to the dynamic phase. For dynamic boundary conditions, tied degrees of freedom were applied along the external sides of the model. Free field boundaries cannot be used because the boundaries in contact with the liquefied material can cause stress concentration and are not compatible with the PM4Sand model (Vilhar et al. 2018). To simulate a rigid base, the "none" option within the dynamic boundary condition was utilized. The corresponding mechanical boundaries at the sides and top were selected to be free, whereas it was fixed at the bottom boundary in Phase II. The PM4Sand material parameters consistent with Basu et al. (2022) were used, as shown in Table 2. The PostShake factor was deactivated ($PostShake = 0$) i.e., reconsolidation was not considered in the second stage.

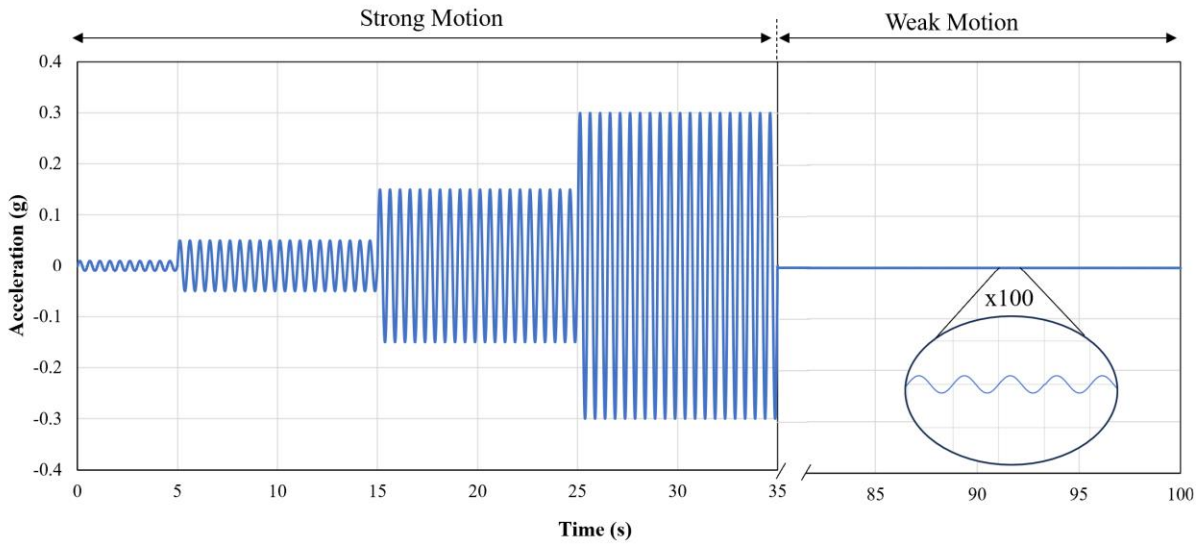

Figure 5. Modified input motion applied at the base of the model.

The third stage (Phase III), the reconsolidation phase, was also analyzed using the "Dynamic with Consolidation" calculation. According to Boulanger & Ziotopoulou (2017), the PostShake factor (see section 3.1.5) must be activated only after the end of strong shaking; hence, the third phase, PM4Sand material model with the $PostShake = 1$ was considered. The remaining weak motion until 100 seconds was applied in Phase III to capture reconsolidation effects as recommended by the Plaxis manual during a post-shaking stage. The boundary conditions used in the third stage are identical to those used in the second stage. In the third stage, the soil is allowed to settle until all pore pressures developed during the strong shaking dissipated. Similarly, in the present study, the hydraulic conductivity was assumed to be constant during the entire simulation. However, in the final phase, the permeability in all zones was increased by 20 folds to reduce the post-shaking calculation time.

Table 3. Summary of simulations in different stages used in Plaxis 2D.

Stages			Initial Phase (1st Stage)	Dynamic Phase (2nd Stage)	Reconsolidation (3rd Stage)
Calculation Type			Gravity loading	Dynamic with Consolidation	Dynamic with Consolidation
Motion			No shaking (Static Equilibrium phase)	Strong Motion	Weak Motion
Boundary Condition	**Hydraulic Boundary**	X_{min}	Closed	Closed	Closed
		X_{max}	Closed	Closed	Closed
		Y_{min}	Closed	Closed	Closed
		Y_{max}	Open	Open	Open
	Mechanical Boundary	X_{min}	Normally Fixed	Free	Free
		X_{max}	Normally Fixed	Free	Free
		Y_{min}	Fully Fixed	Fully Fixed	Fully Fixed
		Y_{max}	Free	Free	Free
	Dynamic Boundary	X_{min}	-	Tied DOF*	Tied DOF*
		X_{max}		Tied DOF*	Tied DOF*
		Y_{min}		None	None
		Y_{max}		Free	Free
PostShake Factor			-	0	1

* DOF: Degrees of Freedom

3.1.4 Validation Results

This section includes the detailed comparison of the Plaxis 2D model (Figure 4) results with the responses of the shake table test experiment and numerical results predicted by the constant hydraulic conductivity model (CK model) of Basu et al. (2022) in FLAC. The locations A, B, & C (shown in Figure 2) were used as reference, where settlement and excess pore pressure were compared.

Figure 6 shows the comparison of the observed time histories of excess pore pressure responses obtained from Plaxis 2D to that of the experiment by Thevanayagam et al. (2009) and the CK model by Basu et al. (2022). The post-liquefaction excess pore pressure dissipation rate predicted by the Plaxis 2D analysis underpredicts the actual data; Plaxis 2D required three times the duration as compared to the actual experimental observation. Basu et al. (2022) also underestimated the rate of dissipation, necessitating six times the actual duration of dissipation than the experimentally observed duration. However, the present study accurately predicts the magnitude of the excess pore pressure.

Figure 7 outlines the comparison of the experimental and simulated settlements. The settlement from the present simulation slightly overestimated the total settlement for the Ottawa F-55 shaking table test by 11%, whereas the CK model of FLAC overestimated the settlement by 20%.

The variations in the rate of dissipation of excess pore pressure can be attributed to the assumption of constant permeability in the numerical models. The difference in results between Plaxis 2D and FLAC models can be attributed to the different numerical methods and mesh settings applied in the two platforms. Overall, and despite these differences, it can be concluded that our numerical model accurately predicts the buildup of excess pore pressure as well as post-liquefaction settlement.

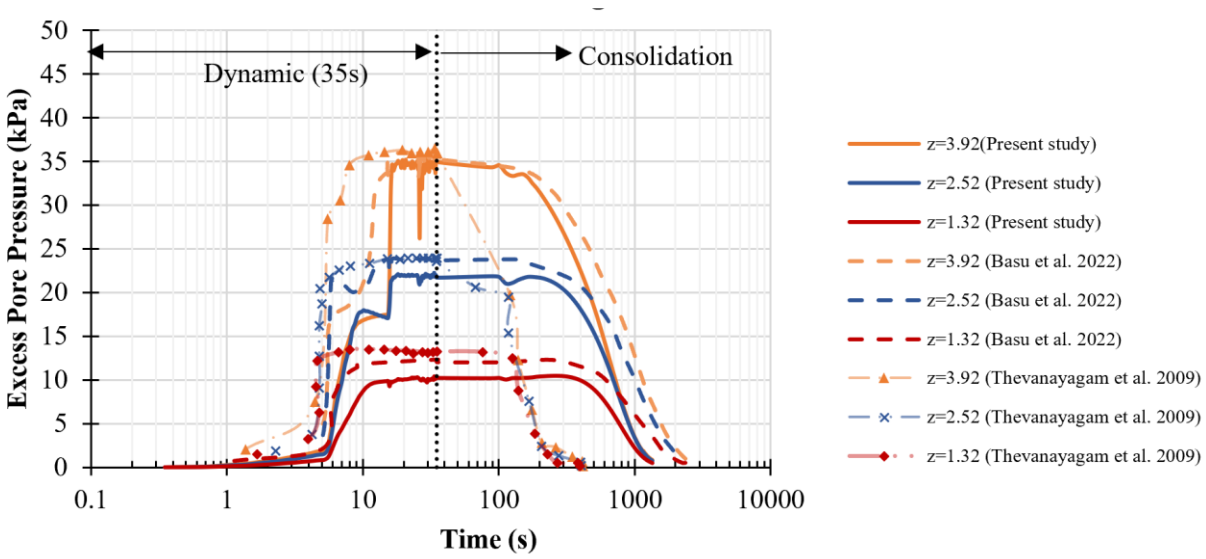

Figure 6. Comparison of excess pore pressure time histories of the experiment, Plaxis 2D model, and FLAC model by Basu et al. (2022)

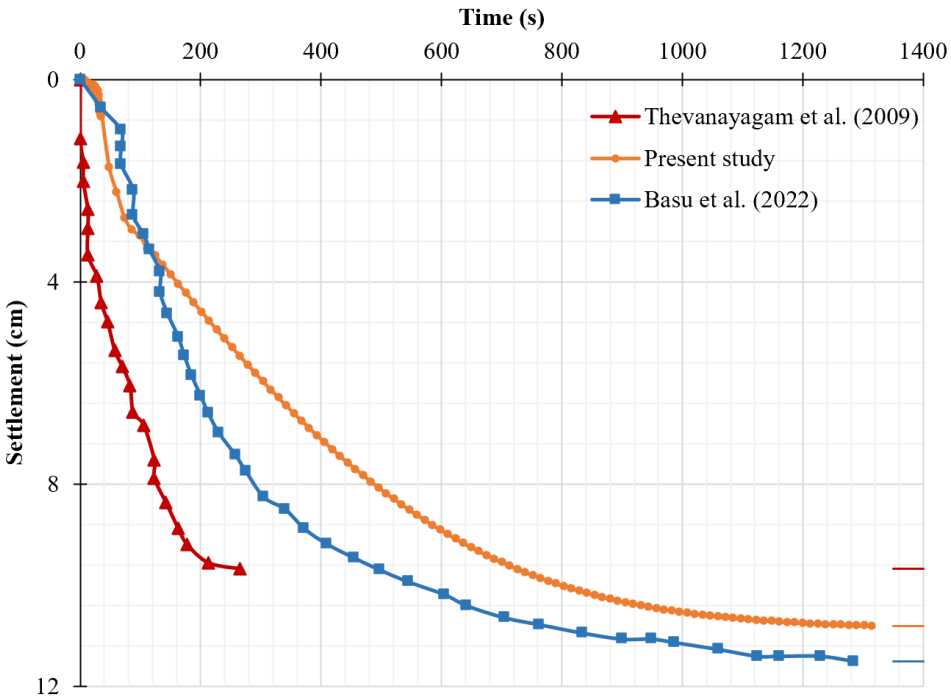

Figure 7. Comparison of settlement time histories of the experiment (Thevanayagam et al. 2009), Plaxis 2D model (Present study), and FLAC model by (Basu et al. 2022). The final observed/predicted settlement is shown as short solid lines at a time of 1400 s.

3.1.5 Preliminary Analysis of the Influence of PostShake Factor

In this section, the model validated in the previous section (Figure 4) was examined by deactivating the PostShake factor ($PostShake = 0$) to have a preliminary assessment of the impact on final settlement when using or not the extended PM4Sand model. The implementation of the PostShake factor was discussed in Section 4.2. The corresponding settlement results obtained with and without activating the PostShake after the main shake are depicted in Figures 8 and 9. It is evident that the conventional PM4Sand (deactivating the PostShake factor) significantly underestimates the post-liquefaction settlement by 75%. Moreover, it underpredicts the time required to dissipate excess pore pressure by a factor of 50. Conversely, activating it leads to a substantial increase in settlement as well as a reduced rate of dissipation. This highlights the crucial role of the extension of PM4Sand towards accurately predicting PostShake reconsolidation settlements.

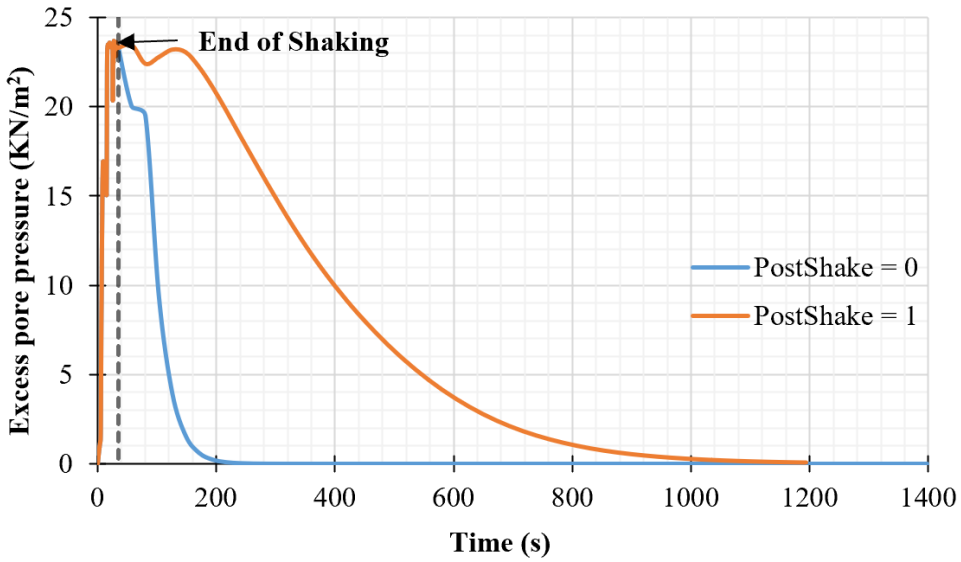

Figure 8. Comparison of excess pore pressure dissipation for cases when PostShake = 0 and PostShake = 1 activated at the end of main shake.

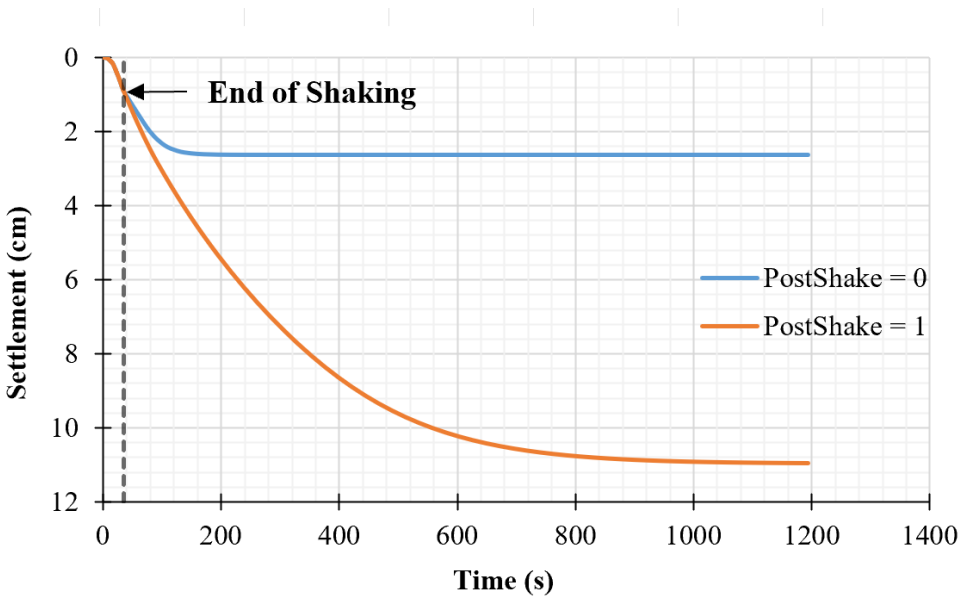

Figure 9. Comparison of settlement for cases when PostShake = 0 and PostShake = 1 (factor activated at the end of the main shake).

3.1.6 Preliminary Analysis to Assess the Effects of Stone Columns

Following a thorough validation process and the analysis of the influence of the PostShake factor, two stone columns were added to the natural ground model (Figure 4), as shown in Figure 10. During this process, two stone columns, each 1m in diameter and 4m long, were introduced to the natural ground at a spacing of 2 m in the third phase (i.e., after the dynamic phase) to have a preliminary assessment of the performance of a reinforced model. The dimensions and spacing of stone columns were based on Poorooshasb and Meyerhof (1997). Stone columns were simulated using a Mohr-Coulomb model with a 37° friction angle, zero cohesion (0 kPa), and permeability of 0.26 cm/s as shown in Table 4. The stone columns were assumed to have a shear modulus seven times higher than the soil. These stone column parameters were adopted from Gingery (2019).

Firstly, it curtailed settlement to some extent, i.e., the settlement was reduced by 15% in contrast to the experimental results, whereas, comparing the settlement of natural ground and reinforced ground obtained from numerical analysis, the settlement was reduced by 30%, as shown in Figure 11. Moreover, from Figure 12, it can be observed that the excess pore pressure dissipates quickly in the reinforced ground with stone columns, given the larger permeability of the reinforced material. This signifies an improved ability of soil to regain stability after experiencing seismic forces. In this regard, the study of stone columns and their impact in reducing reconsolidation settlement is further detailed in the following sections.

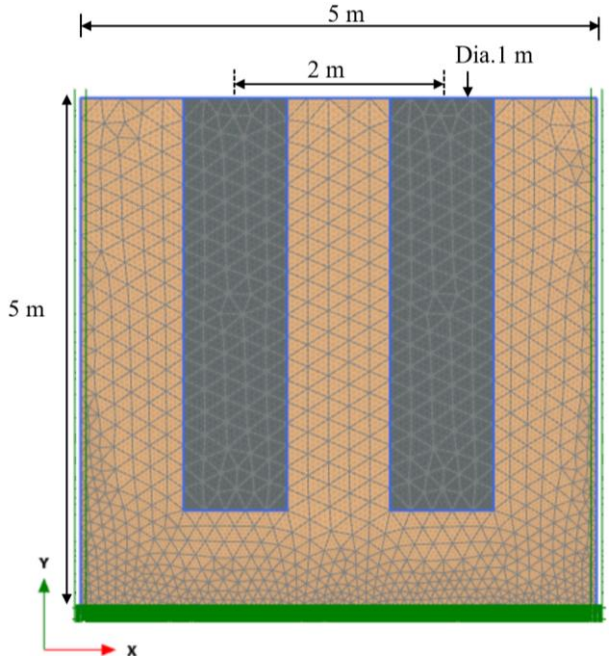

Figure 10. Typical Plaxis 2D meshes after the inclusion of stone columns in Ottawa F-55 natural ground (Thevanayagam et al. 2009).

Table 4. Summary of stone column parameters.

Material	Unit weight, γ (KN/m3)	Friction Angle, $\phi°$ *	Cohesion, c (kPa)	Permeability, k (cm/s) *	Shear Modulus, G (kPa)	Poisson ratio, ν *
Stone Column	19.65	37	0	0.26	1.13×10^5	0.3

* These parameters of stone columns were taken from Gingery (2021).

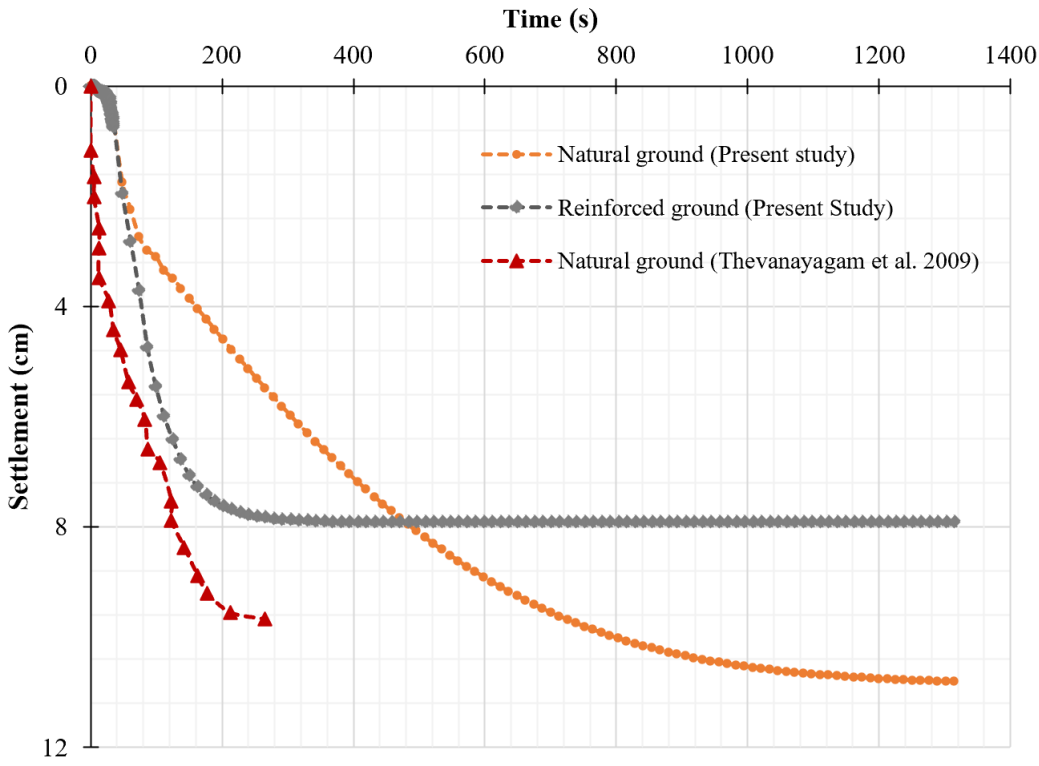

Figure 11. Comparison of settlement time histories of an experiment, natural ground modeled in Plaxis 2D , and reinforced ground modeled in Plaxis 2D.

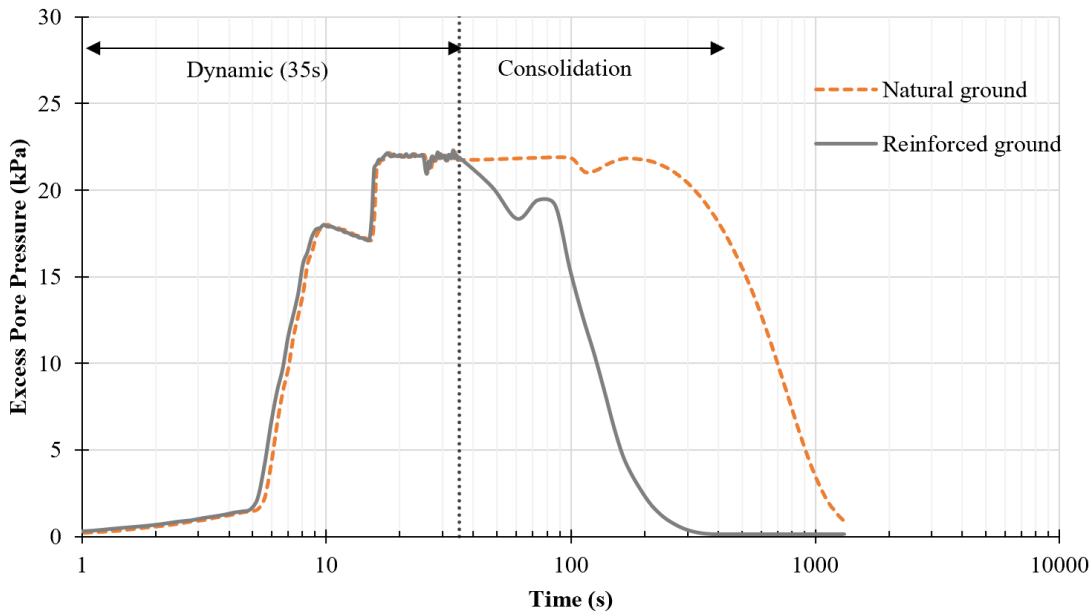

Figure 12. Comparison of excess pore pressure time histories of natural ground and reinforced ground modeled in Plaxis 2D.

3.2 Numerical Model for Parametric Analyses

In the present study, a theoretical numerical model was generated based on the one used for validation purposes to investigate the effectiveness of stone columns in mitigating liquefaction-induced settlements when subjected to real ground motions, especially emphasizing reconsolidation settlement. The dynamic and post-shaking responses of the natural ground (without stone columns) and reinforced ground (with stone columns) were simulated under a plane strain formulation using Plaxis 2D. As a benchmark model, the soil profile of the 10m x 20 m configuration was considered, as shown in Figure 13. The disturbances along the interface between the stone column and soil, as well as the spatial variations of natural soil along lateral and vertical directions, were not modeled. Additionally, any relative displacement between the stone columns and the surrounding soil was not taken into account. The groundwater table was considered to be at the top of the model, and the bottom boundary was assumed to be impermeable.

The analyses were conducted in three distinct phases identical to the stages of the numerical framework validation simulation, as shown in Table 3. The primary parameters used in this study are also identical to those used in the validation section, in Table 2 (Ottawa F-55 sand). Although recent research has indicated that the changes in secondary parameters ($e_{max}, e_{min}, n^d, n^b, \phi_{cv}, \nu, Q, and\ R$) can impact the model performance, the present study opts for default values for these parameters.

The improved soil profile includes four 8m long stone columns with a diameter of 1m that are spaced at 3m center-to-center, as shown in Figure 14. The spacing (S) to diameter (D_c) ratio of 3 was used for the present analysis (Clemente et al. 2005). The properties of the stone column used in this study are summarized in Table 4.

In this study, three models were analyzed: (a) “natural ground” (model without stone columns), (b) “reinforced ground from Phase I” (the stone columns were activated right from the initial phase of the simulation), and (c) “reinforced ground from Phase III” (the stone columns were only activated in the final reconsolidation phase after a liquefaction event had occurred in the natural ground.) This distinction in modeling was carried out for two purposes. The “reinforced ground from Phase III” allows for the examination of the effect of stone columns after the liquefaction triggering of the natural ground i.e., this model and natural ground are both subjected to the same excess pore pressure, so given the same pore pressure ratio (r_u), the

improvement provided by stone columns after the end of shaking is assessed. In contrast, the "reinforced ground from Phase I" model facilitates the assessment of the impact of stone columns right from the beginning of shaking, providing valuable insights into their effectiveness in preventing liquefaction triggering as well as post-liquefaction settlements.

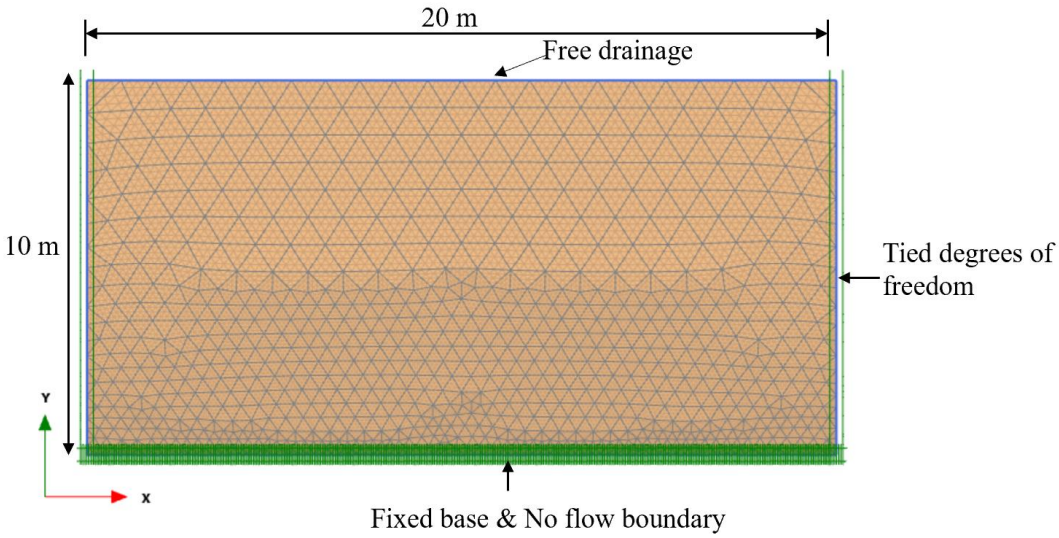

Figure 13. Plaxis 2D mesh of the proposed natural ground model.

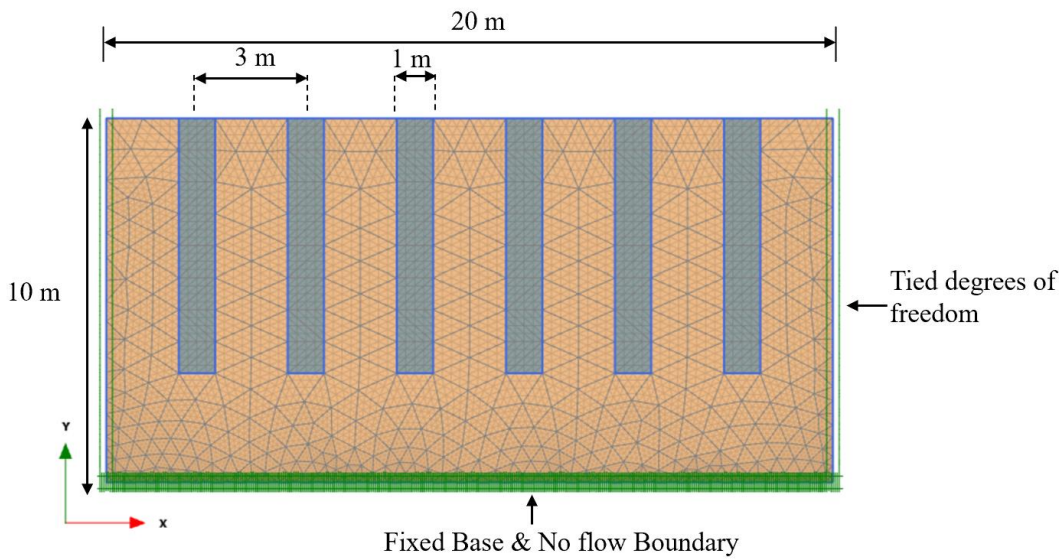

Figure 14. Plaxis 2D mesh of the proposed reinforced ground model.

Chapter 4

Numerical Results

4.1 Parametric Analysis

A comprehensive investigation across a spectrum of ground motions and ground motion intensities was carried out to understand how stone columns impact the mitigation of reconsolidation settlement after liquefaction. This involved subjecting all three models, i.e., natural ground, reinforced ground from Phase I, and reinforced ground from Phase III models to 12 input motions, each recorded from different events of varying magnitudes. These motions exhibited a wide range of Peak Ground Acceleration (PGA), maximum pseudo-spectral acceleration value ($S_{a,max}$), and Arias Intensity (I_A) as outlined in Table 5. The pseudo-spectral acceleration response spectra of these motions are shown in Figure 15. This parametric analysis was performed to discern the effects of stone columns under different seismic loadings.

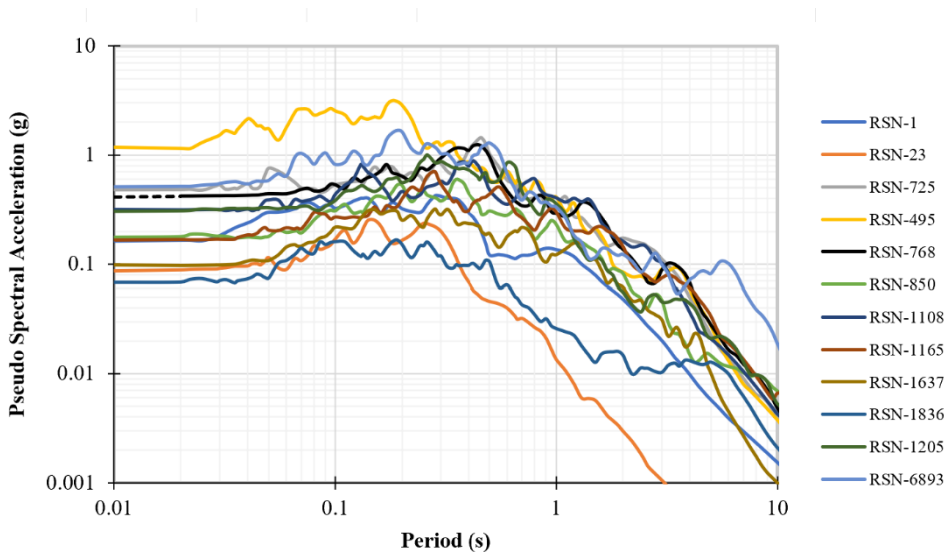

Figure 15. Pseudo-spectral response spectra at a damping ratio of 5% of the ground motions.

Table 5. Details of ground motions based on PEER NGA-West2 Database (Ancheta et al. 2014).

S. N.	Earthquake	Year	Station	RSN*	Magnitude (M_w)	Parameters of input motion		Parameters at the soil surface	
						PGA* (g)	I_A* (m/s)	PGA* (g)	I_A * (m/s)
1	Helena_ Montana-01	1935	Carroll College	1	6	0.16	0.01	0.020	0.01
2	San Francisco	1957	Golden Gate Park	23	5.28	0.09	0.02	0.032	0.02
3	Nahanni_ Canada	1985	Site 1	495	6.76	1.18	3.88	0.098	0.14
4	Loma Prieta	1989	Gilroy Array #4	768	6.93	0.42	1.1	0.067	0.17
5	Landers	1992	Desert Hot Springs	850	7.28	0.18	0.67	0.066	0.12
6	Kobe_ Japan	1995	Kobe Universit y	1108	6.9	0.31	0.81	0.058	0.31
7	Kocaeli_ Turkey	1999	Izmit	1165	7.51	0.17	0.56	0.093	0.24
8	Manjil_ Iran	1990	Rudsar	1637	7.37	0.10	0.32	0.062	0.18
9	Hector Mine	1999	Twentyni ne Palms	1836	7.13	0.07	0.06	0.059	0.23
10	Darfield_ New Zealand	2010	DFHS	6893	7	0.51	2.82	0.075	0.39
11	Superstition Hills-02	1987	Poe Road (temp)	725	6.54	0.48	2.12	0.044	0.08
12	Chi Chi_Taiwan	1999	CHY041	1205	7.62	0.30	1.54	0.083	0.37

*RSN: Regional Seismic Network
*PGA = Peak Ground Acceleration
*I_A = Arias Intensity

Figures 16 (a) and (b) show that the r_u values at each point within the model, are different and a consistent trend was observed across other models. Hence, r_u values reported in this study for each model characterize the modal values, representing the most frequently occurring r_u values within the upper 4 meters of the model and within the middle section of the model. In particular, the computation of modal r_u values exclude a 2-meter section on each edge of the model to minimize boundary effects.

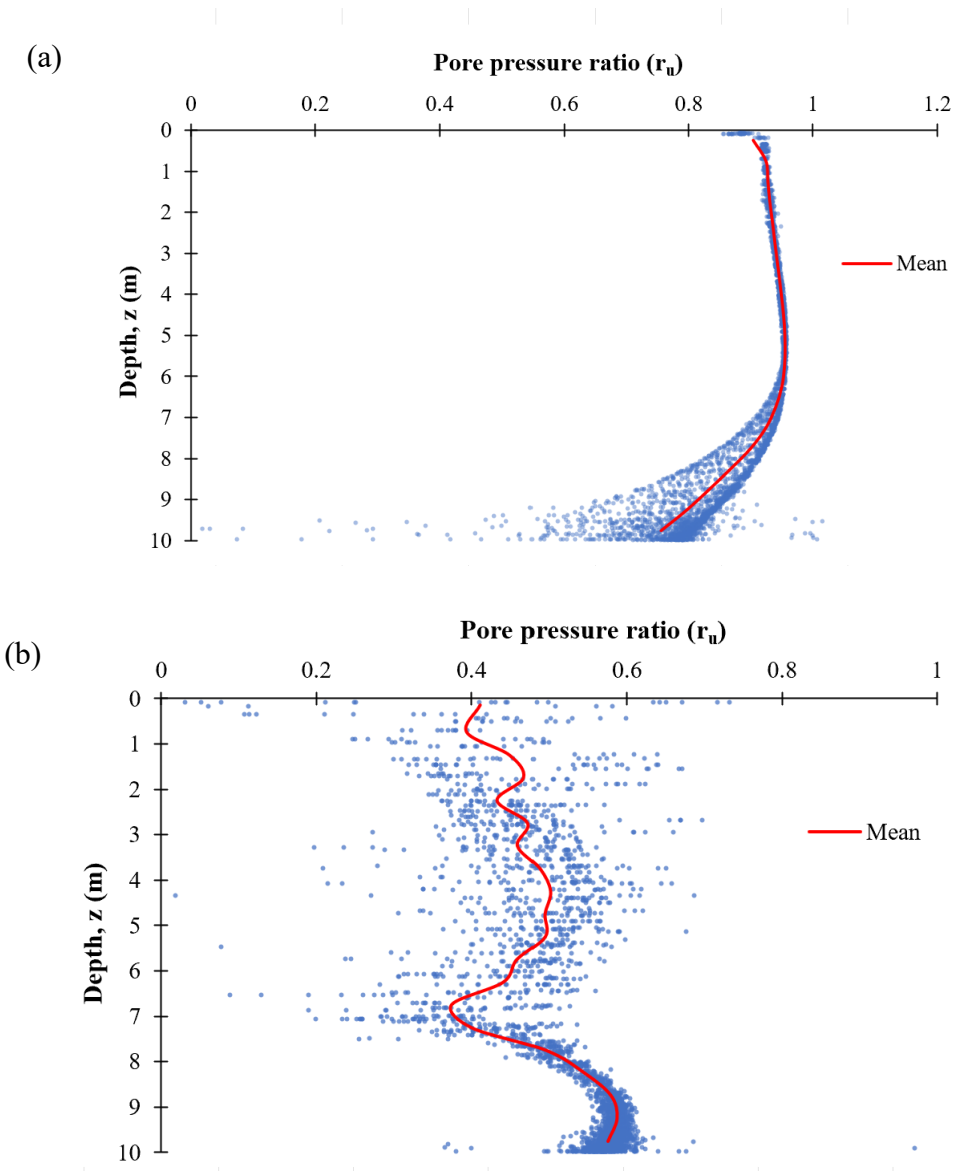

Figure 16. Distribution of pore pressure ratio as a function of depth (m) for (a) natural ground condition and (b) reinforced ground from Phase I, both subjected to the Superstition Hills 02 ground motion.

Table 6 shows a summary of the maximum values of reconsolidation settlement and the corresponding pore pressure ratio (r_u) for natural ground, reinforced ground from Phase I, and reinforced ground from Phase III across different ground motions. These results are discussed in detail in the discussions below and presented in the figures therein.

Table 6. Comparison of pore pressure ratio and reconsolidation settlement for Natural Ground vs Reinforced Ground (from Phase I and Phase III) for all input motions.

S. No.	Event name	Arias Intensity (I_A) (m/s)	Natural Ground		Reinforced Ground from Phase I		Reinforced Ground from Phase III	
			r_u	Settlement (cm)	r_u	Settlement (cm)	r_u	Settlement (cm)
1	Helena_ Montana-01	0.01	0.02	0.05	0.01	0.04	0.02	0.04
2	San Francisco	0.02	0.043	0.09	0.01	0.09	0.043	0.07
3	Nahanni_ Canada	3.88	0.94	20	0.88	17	0.94	17.4
4	Loma Prieta	1.1	0.88	3.3	0.17	1.9	0.88	2.2
5	Landers	0.67	0.85	4.1	0.09	3	0.85	3
6	Kobe_ Japan	0.81	0.93	17.5	0.56	5.1	0.93	11.6
7	Kocaeli_ Turkey	0.56	0.91	7.5	0.54	4.1	0.91	5.1
8	Manjil_ Iran	0.32	0.89	3.5	0.1	0.7	0.89	2
9	Hector Mine	0.06	0.08	0.2	0.01	0.2	0.08	0.2
10	Darfield_ New Zealand	2.82	0.94	31	0.85	22	0.94	22
11	Superstition Hills-02	2.12	0.94	19	0.46	5.4	0.94	12.9
12	Chi Chi Taiwan	1.54	0.94	21.9	0.64	10	0.94	12.9

The pore pressure ratio was studied as a function of various Intensity Measures (IMs) of the input motions – Arias Intensity (I_A), $PGA, S_{a,max}, Duration$, etc. Only I_A was able to separate the cases of liquefaction vs. no liquefaction for both the reinforced and the natural ground. Figure 17a shows the comparison of the pore pressure as a function of the I_A of the input motion. Shaded regions within the plot signify areas where data availability is limited, resulting in increased uncertainty regarding the liquefaction status of those particular regions. Assuming $r_u \geq 0.8$ indicates liquefaction triggering (Thum et al. 2022), the results shown in Figure 17a present three scenarios: a) $I_A < 0.3\ m/s$, liquefaction is not triggered for either the natural or reinforced ground, b) $0.3\ m/s < I_A < 2.3\ m/s$, liquefaction is triggered for natural ground but not for reinforced ground conditions, and c) $I_A > 2.8\ m/s$, liquefaction occurs for both natural and reinforced ground conditions. As previously mentioned, $2.3\ m/s < I_A < 2.8\ m/s$ is the uncertainty region because of the lack of data within the region. In all of these cases, the

inclusion of stone columns reduces r_u by an average of 57% and 30% for $0.3\ m/s < I_A < 2.3\ m/s$ and $I_A > 2.8\ m/s$, respectively. From Figure 17a, it is observed that the pore pressure ratio is as high as 0.85 and 0.88 for I_A 2.82 m/s and 3.88 m/s, respectively even under the reinforced ground condition. There is a 9% and 6% reduction of pore pressure ratio for I_A : 2.82 m/s and 3.88 m/s, respectively.

The pore pressure ratio (r_u) at the end of shaking is correlated to Arias Intensity (I_A). In particular, I_A has been selected as it reflects two crucial aspects of ground motion: amplitude and duration (Kramer 1996). Based on previous studies, it is evident that I_A is an effective measure of representing ground motion intensity that can capture record-to-record variations of seismic-induced settlements (Cascone et al. 2021; Chakraborty and Sawant 2022; Huang and Wang 2017; Wang 2012).

Moreover, since the trends observed could be highly a function of profile characteristics, the pore pressure was also studied as a function of IMs at the ground surface: I_A, PGA, $S_{a,max}$, and PGA at the ground surface normalized by the Magnitude Scaling Factor (MSF). In this study, atlernatively, PGA at the ground surface normalized by MSF is denoted by $PGA_{7.5}$. The Magnitude Scaling Factor (MSF) was evaluated using the equation provided by Boulanger and Idriss (2014):

$$MSF = 1 + (MSF_{Max} - 1)\left\{8.64exp\left(\frac{-M_w}{4}\right) - 1.325\right\} \leq 2.2 \tag{12}$$

$$MSF_{Max} = 1.09 + \left(\frac{q_{c1NCS}}{180}\right)^2 \leq 2.2 \tag{13}$$

where q_{c1NCS} is the normalized cone penetration resistance and M_w is the moment magnitude.

Among these IMs, PGA at the ground surface and $PGA_{7.5}$ were able to capture the separation of cases of liquefaction for both natural and reinforced ground as illustrated in Figures 17b and 17c. For instance, when a) $PGA\ at\ the\ ground\ surface < 0.042g$, liquefaction is not triggered for either the natural or reinforced ground, b) $0.042g < PGA < 0.082g$, liquefaction is triggered for natural ground but not for reinforced ground conditions, and c) $PGA > 0.082g$, liquefaction occurs for both natural and reinforced ground conditions as shown in Figure 17c. Shaded regions within the plot indicate the areas where data availability is limited.

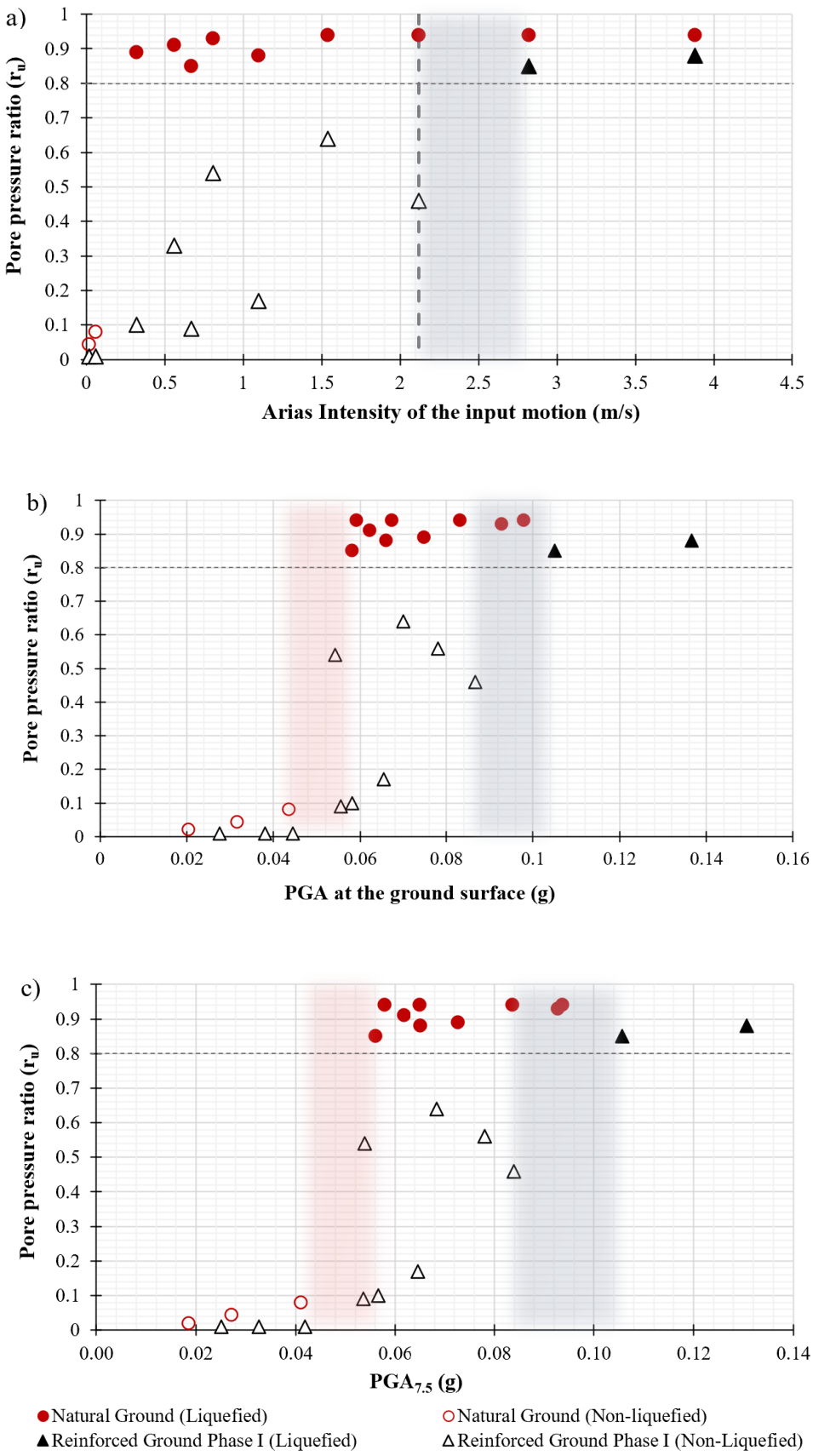

Figure 17. Pore pressure ratio as a function of (a) Arias Intensity (I_A) of the input motion, (b) PGA at the ground surface, and (c) $PGA_{7.5}$.

Figure 18 compares the PGA at the ground surface for the natural ground and that for the reinforced ground for all 12 motions. This figure shows that the PGA is amplified at the ground surface when stone columns are added for most of the motions. A similar trend was also observed in the case of $PGA_{7.5}$ for the natural ground and the reinforced ground.

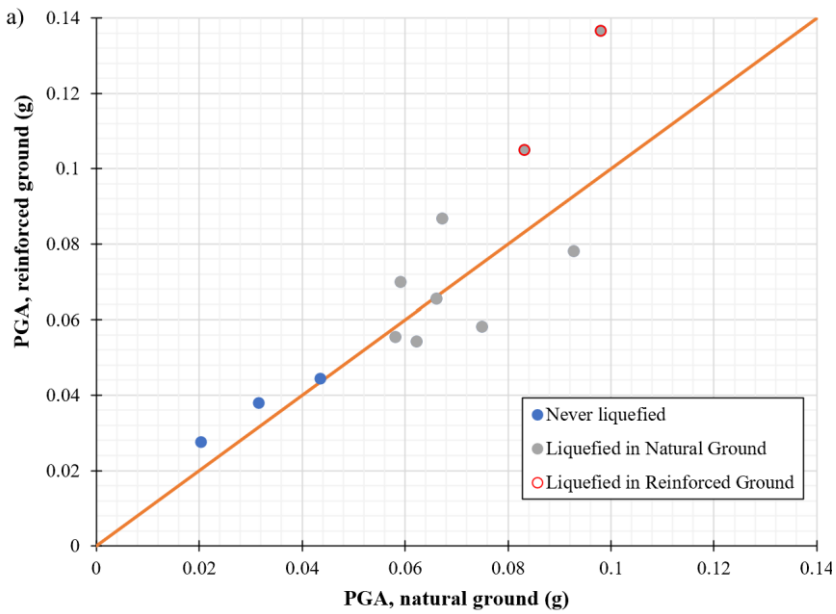

Figure 18. PGA at the ground surface for the natural ground and that for the reinforced ground.

Figure 19 depicts the final settlement as a function of three Intensity Measures (IMs) of the input motion: I_A, $S_{a,max}$, and PGA for the natural ground, reinforced ground from Phase I, and reinforced ground from Phase III models measured at the centerline in between two stone columns at the surface. Different trends were fitted for all three IMs; however, the polynomial trend proved to be the most optimal. The best fit was observed in the case of I_A of the input motion with the highest R-squared value. Therefore, I_A of the input motion, is considered an optimal indicator for assessing the effectiveness of liquefaction mitigation in further analyses. It can be inferred from Figure 19a that settlement rises with an increase in Arias Intensity up to a certain threshold. For instance, the Darfield ground motion ($I_A = 2.82\ m/s$) resulted in a maximum final surface settlement of 31 cm, whereas Nahanni, with comparatively higher $I_A = 3.88\ m/s$, generated relatively a lower settlement of 20 cm. This can be attributed to Darfield's higher significant duration ($D_{5-95} = 22s$) than that of Nahanni ($D_{5-95} = 7.9s$), highlighting the critical role of prolonged shaking in settlement results, not directly captured by I_A. Another reason could be the difference in predominant frequency values of different motions.

Overall, the inclusion of stone columns from Phase I has the highest impact on mitigating overall settlement. This can be attributed to the increased rate of dissipation of pore pressure right from the dynamic phase (Figure 22), which prevents the development of excess pore pressures, combined with the increased stiffness of the columns, which reduces shear strains.

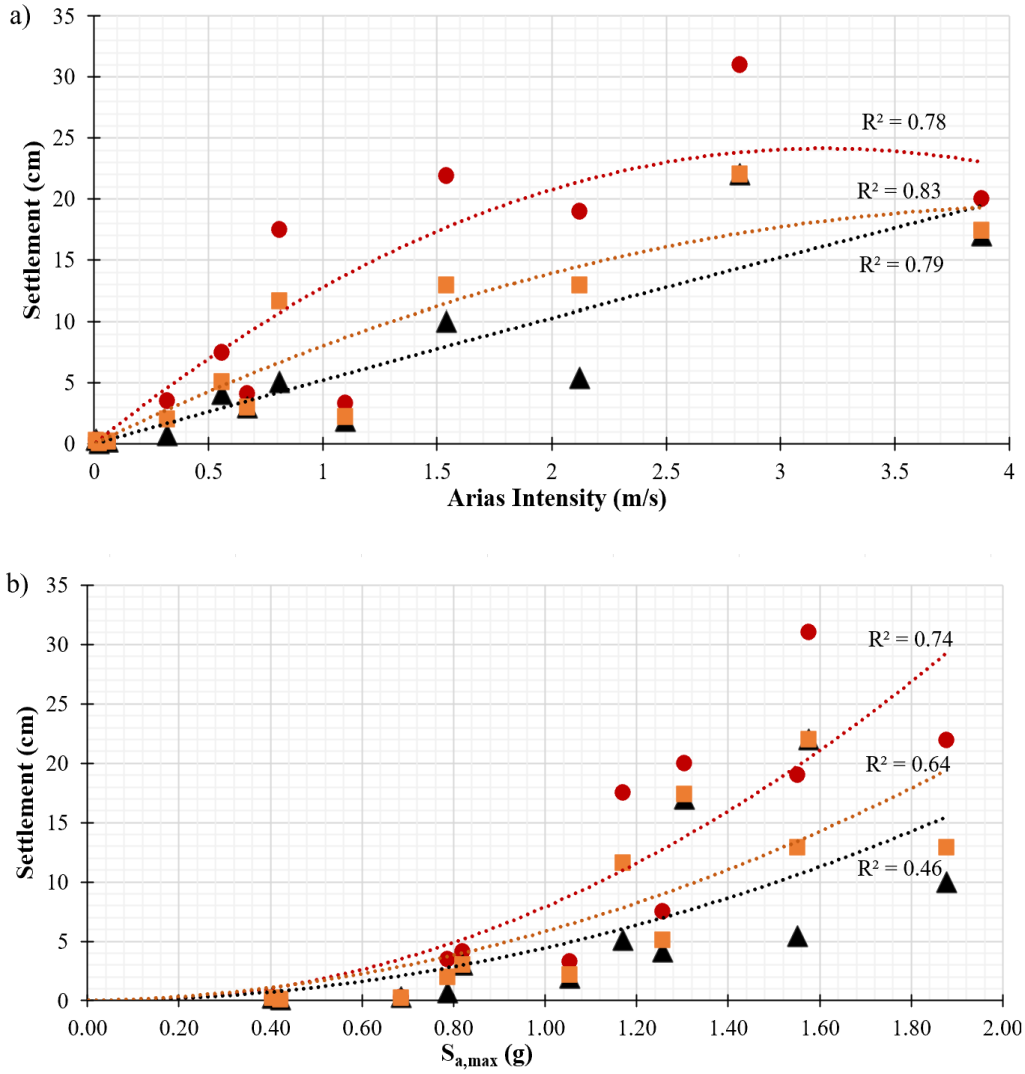

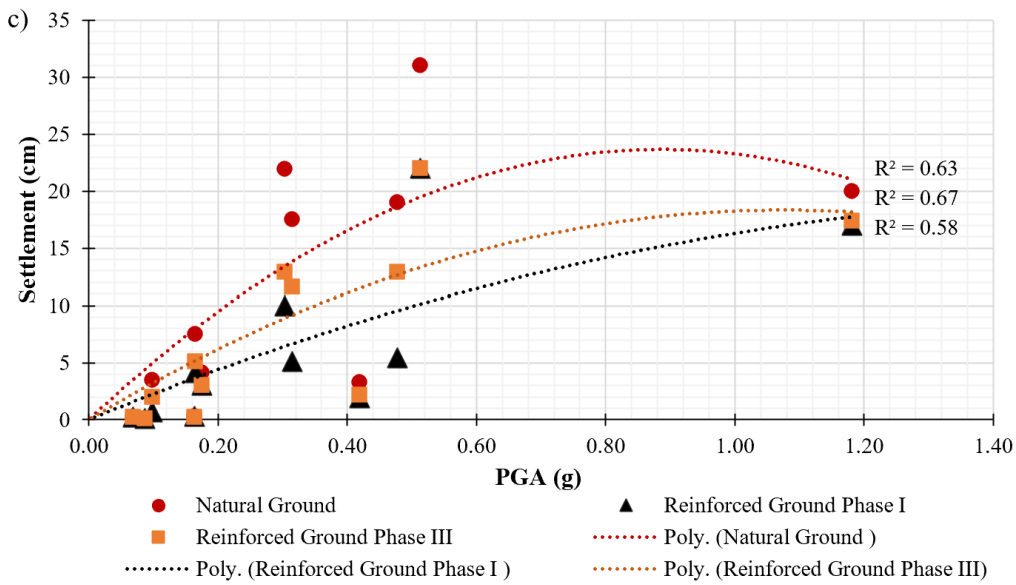

Figure 19. The settlement as a function of (a) I_A, (b) $S_{a,max}$, and (c) PGA measured at the centerline in between two stone columns at the surface of the soil model.

Figure 20 illustrates the relationship between settlement (measured at the centerline between two stone columns) and pore pressure ratio (r_u) using the I_A of input motions presented in Table 6. The graph shows that an increase in pore pressure ratio corresponds to a notable increase in settlement for both natural and reinforced ground. As r_u increases, it signifies a greater buildup of pore pressure within the soil. This elevated pore pressure has a substantial impact on settlement, causing an upward trend in the settlement values observed. A comparative examination of settlement between natural ground and reinforced ground from Phase I indicates an average reduction of 49% while a corresponding reduction of 30% is observed in the case of reinforced ground from Phase III excluding the cases where there was no liquefaction triggering (r_u < 0.8) in the natural ground condition. Furthermore, Figure 20 illustrates two cases that liquefied in both conditions: natural ground and reinforced ground from Phase I. The depiction indicates that while liquefaction is not entirely prevented in the reinforced condition, there is a discernible reduction in settlement.

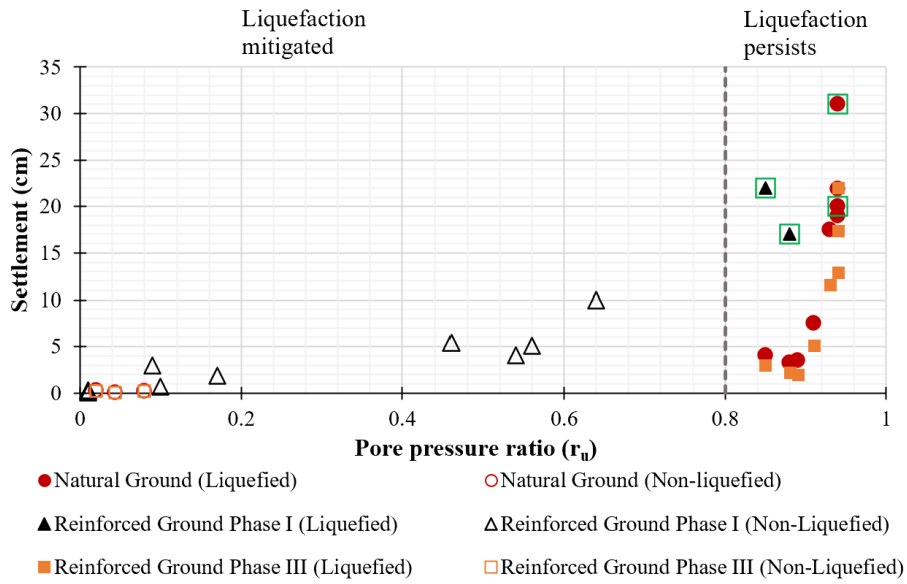

Figure 20. Settlement as a function of pore pressure ratio measured at the centerline in between stone columns at the surface of the soil model.

Figure 21 shows the post-liquefaction settlement time histories for different earthquake motions that yielded liquefaction triggering, defined herein as $r_u \geq 0.8$, in natural ground conditions. It also illustrates the comparison of the rate of settlement developed for natural ground, reinforced ground from Phase I, and reinforced ground from Phase III. The introduction of stone columns curtails settlement substantially. Figure 22 compares excess pore pressure developed over dynamic time for natural ground, reinforced ground from Phase I, and reinforced ground from Phase III, for the same set of input motions as in Figure 21. The time required to dissipate excess pore pressure is reduced by 8 folds on average after introducing stone columns from Phase I. Moreover, even after including the stone columns following dynamic loading (Phase III), the time required for excess pore pressure dissipation decreased by 5 folds. Hence, by maintaining effective drainage pathways and reinforcing the soil structure, stone columns curtailed the development of critical pore pressure conditions during seismic events. This effect can only be maintained if the stone columns maintain a high hydraulic conductivity after installation. Reduction of hydraulic conductivity can occur from particle migration into the stone columns. Thus, caution is recommended in using stone columns for liquefaction mitigation.

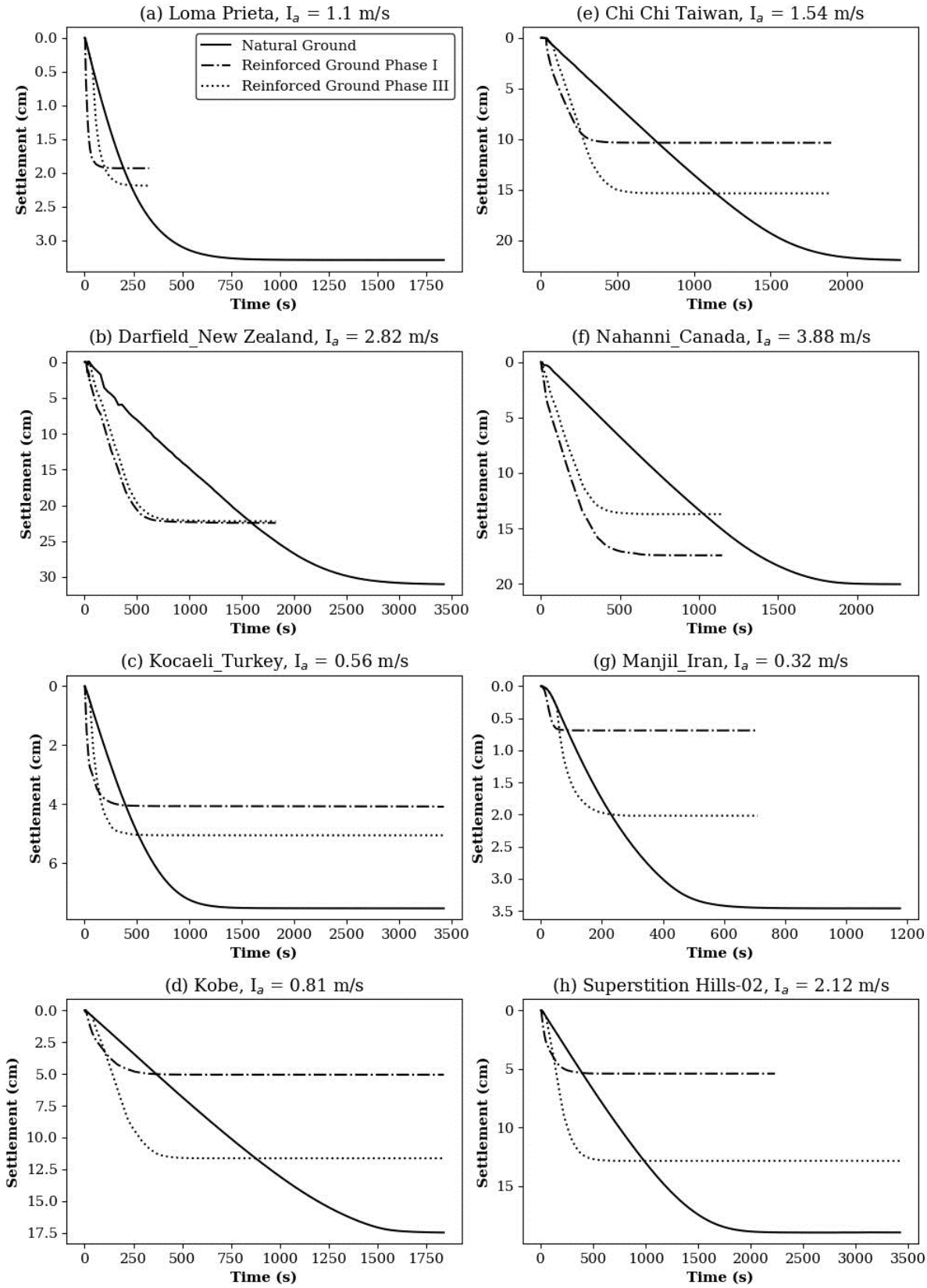

Figure 21. Settlement time histories for earthquake motions that caused liquefaction ($r_u \geq 0.8$).

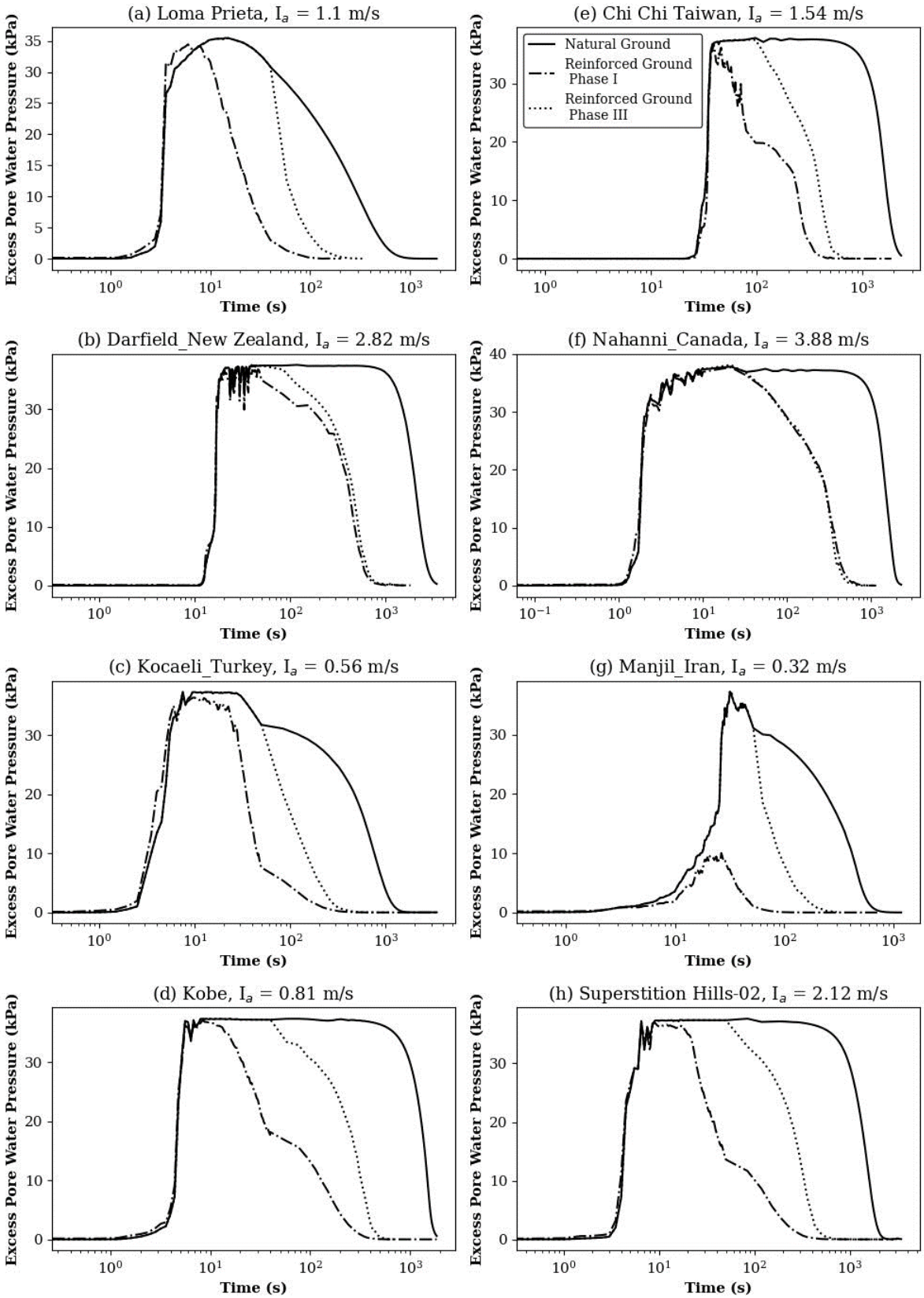

Figure 22. Excess pore pressure time histories for earthquake motions that caused liquefaction ($r_u \geq 0.8$).

4.2 PostShake Analysis

Three additional calculations were performed to study the sensitivity of the results on the PostShake parameter when it remains deactivated (i.e., 0) throughout the calculation, and the extension in PM4Sand to account for post-liquefaction is not considered. The simulations were performed using the acceleration time histories from (Table 5): Kobe_Japan ($I_A = 0.81\ m/s$), Superstition Hills-02 ($I_A = 2.12\ m/s$), and Chi Chi_Taiwan ($I_A = 1.54\ m/s$) earthquakes. These motions were selected because they produced substantial settlements as shown in Table 6. The results have been compared with their counterparts presented in section 4.1 (in which the PostShake parameter is set to 1 during Phase III).

Figure 23 illustrates the effect of the PostShake factor under natural ground and reinforced ground conditions from Phase I and Phase III. It is clear that deactivating this factor significantly underestimates the post-liquefaction settlement. For all three ground motions, the PostShake factor = 0 analysis results in the underestimation of post-liquefaction settlements in the natural ground and the reinforced ground from Phase III models by approximately 80% in comparison to the PostShake = 1 analysis. On the other hand, in the reinforced ground from the Phase I model, on deactivating the PostShake factor, the settlement is underestimated by approximately 27% for all three motions. It can be inferred that the underestimation of the settlement in the reinforced ground from the Phase I model is small in comparison to the other two models. This can be due to the stabilizing effect of stone columns that plays a crucial role in influencing settlement behavior during and after seismic events. The dissipation of excess pore pressure initiated by stone columns during Phase I might have contributed to maintaining a relatively low r_u. Hence, toggling the PostShake factor in the case of reinforced ground from Phase I does not induce significant changes in the settlement as the model has been stabilized against potential post-liquefaction settlement effects due to the inclusion of stone columns.

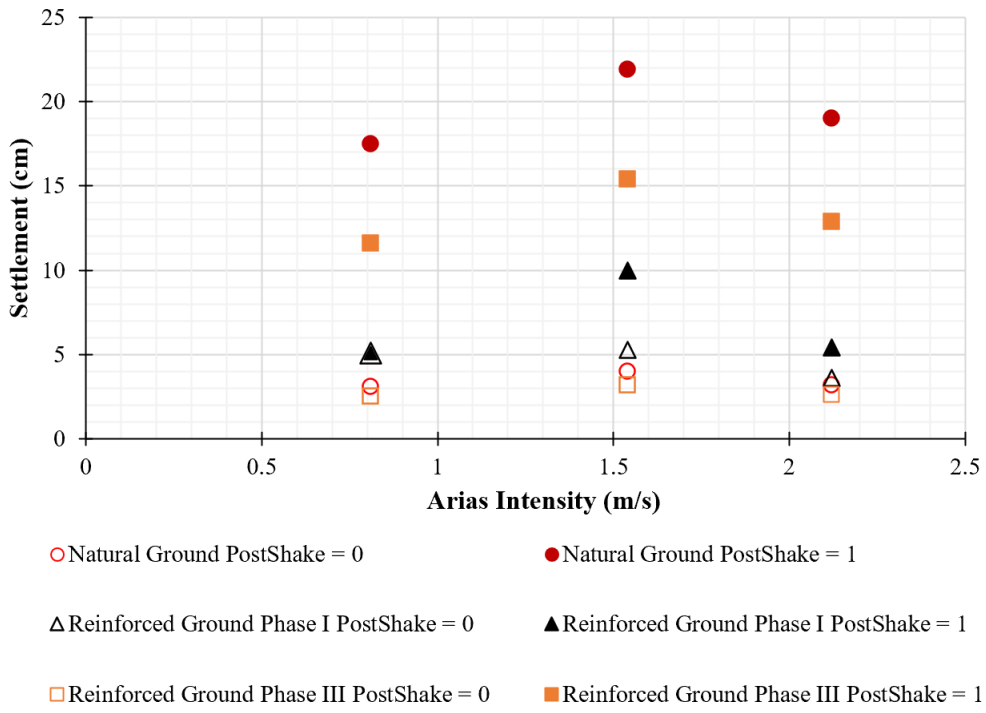

Figure 23. Comparative Study of Settlement in Natural Ground, Reinforced Ground (Phase I and III) with and without PostShake factor subjected to different motions.

4.3 Analysis with footing

As presented in Table 6, motions characterized by low Arias Intensity (I_A) did not result in a significant amount of settlement under dynamic loading in free field conditions. Consequently, the expected enhancement in the corresponding reinforced ground was not discernible. Hence in order to better capture the impact of stone columns in these cases, the footing load was applied as shown in Figure 24. To achieve this, six motions with low I_A, i.e., Helena_Montana-01 ($I_A = 0.01\, m/s$), San Francisco ($I_A = 0.02\, m/s$), Hector Mine ($I_A = 0.06\, m/s$), Manjil_Iran ($I_A = 0.32\, m/s$), Kocaeli (($I_A = 0.56\, m/s$), and Landers ($I_A = 0.67\, m/s$) were selected. A centered baseplate of 3m wide and a line load of 24kN/m/m were added in the three models (i.e., natural ground, reinforced ground from Phase I, and reinforced ground from Phase III) to replicate the footing load. The phases used in the numerical model with footing are shown in Table 7.

Table 8 presents the pore pressure ratio (r_u) developed after the end of shaking for five motions with and without footing load. No instances of initiation of liquefaction triggering were observed, even in the presence of footing load, for three earthquake motions with the lowest

I_A (i.e., Helena_ Montana-01, San Francisco, and Hector Mine). Hence, a detailed comparison of reconsolidation settlement of earthquake motions (Manjil_Iran ($I_A = 0.32\ m/s$), Kocaeli ($I_A = 0.56\ m/s$), and Landers ($I_A = 0.67\ m/s$)) that triggered the onset of liquefaction ($r_u \geq 0.8$) in natural ground conditions with surcharge load, is presented in Figure 25.

When the footing load is included in the natural ground model, the settlement increases. Provided the same r_u, the settlement increase for natural ground and reinforced ground from Phase III models are very similar (10% smaller with stone columns) i.e., the effect of stone columns is significantly less pronounced in this case. On the other hand, when the benefits of the stone columns are also considered during the strong shaking (ground reinforcement from Phase I), the settlement is substantially reduced, i.e., the settlement decreased by approximately 70% on average compared to the natural ground with footing. These results highly emphasize the efficiency of installing stone columns, especially under footing loads, to minimize post-liquefaction settlement. This is primarily because liquefaction triggering is prevented (i.e., r_u does not rise to 0.8) with the inclusion of stone columns. However, in the case of the Kocaeli earthquake with $I_A = 0.56\ m/s$, the reduction of settlement is only 29% i.e., not as high as the other two cases, this might be due to the comparatively high magnitude and significant duration of the motion.

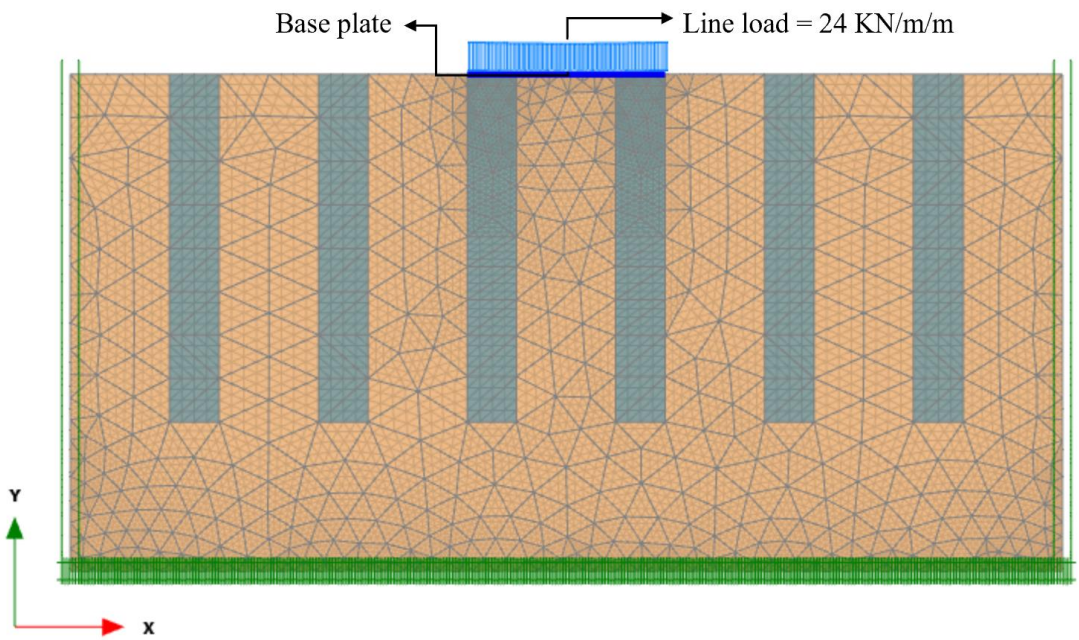

Figure 24. Plaxis 2D mesh of the reinforced ground model with footing load on top.

Table 7. Calculation stages used in the numerical model with footing load in Plaxis 2D.

Phase	Phase name	Loading	Phase description
I	Initial phase	Footing	Calculation of initial geometry and initializing stresses,
II	Stabilizing phase	Footing	Plastic phase to reset displacements, strains to ensure equilibrium in the computation of initial stress field
III	Dynamic phase	Footing + Strong Motion	Input earthquake motion and generation of excess pore pressure
IV	Reconsolidation phase	Footing +Weak Motion	Dissipation of excess pore pressure

Table 8. Summary of r_u with and without footing load corresponding to the motions with low I_A.

No.	Earthquake	I_A (m/s)	Pore pressure ratio (r_u)			
			Without footing load		With footing load	
			Natural Ground	Reinforced Ground Phase I	Natural Ground	Reinforced Ground Phase I
1	Helena_ Montana-01	0.01	0.02	0.01	0.18	0.09
2	San Francisco	0.02	0.043	0.01	0.54	0.36
3	Hector Mine	0.06	0.08	0.01	0.35	0.1
4	Manjil_ Iran	0.32	0.89	0.1	0.9	0.3
5	Kocaeli	0.56	0.91	0.54	0.91	0.7
6	Landers	0.67	0.85	0.09	0.92	0.16

4.3 ANALYSIS WITH FOOTING

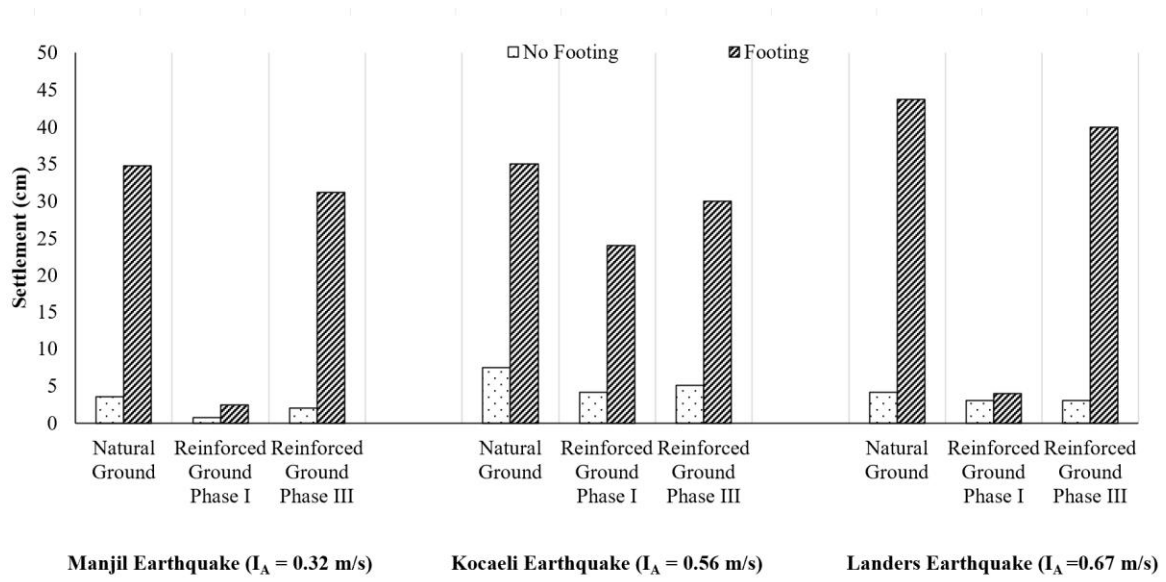

Figure 25. Settlement of natural ground, reinforced ground (Phase I and Phase III) under free field condition (without footing) and with footing load when subjected to (a) Manjil_Iran, (b) Kocaeli_Turkey, and (c) Landers earthquake.

Chapter 5

Summary and Future Work

5.1 Conclusions

The liquefaction behavior of Ottawa F-55 sand was investigated using the user-defined constitutive model PM4Sand, available in the finite element program Plaxis 2D. A shake table test by Thevanayagam et al. (2009) with the constitutive model calibrated by Basu et al. (2022) was used for the validation of the numerical framework. Overall, the results show a reasonable agreement between numerical predictions and experimental data for liquefaction triggering (in terms of maximum r_u) and post-liquefaction settlement. Furthermore, using the same numerical model, two preliminary assessments were performed on (a) the influence of the PostShake factor in PM4Sand, which showed that the deactivation of the PostShake factor yielded a high underestimation of post-liquefaction settlement, and (b) the effect of including stone columns in the model, which showed a reduced post-liquefaction settlement in the reinforced ground compared to the natural ground.

Subsequently, a theoretical numerical model to study the impact of stone columns on liquefaction response was presented. The numerical analyses employed a 2D fully coupled hydro-mechanical finite element formulation in plane-strain conditions, in both natural and reinforced ground conditions. The reinforced ground conditions were divided into two models: (a) reinforced ground from Phase I (stone columns were added to the model from the beginning of the simulation and before applying the ground shaking) and (b) reinforced ground from Phase III (stone columns were added to the model in the final phase, i.e., post liquefaction). This differentiation in modeling was made to investigate the impacts of stone columns right from the onset of shaking and after the end of shaking. All three soil models were subjected to 12 ground motions, encompassing a large range of earthquake magnitudes, frequencies, and durations. Some key findings of the present study are:

- Several existing liquefaction models, such as SANISAND (2010), WANG2D (2014), UBCSand (2011), and PM4Sand (2013), have been expanded to capture post-

liquefaction behavior. These models address reconsolidation response by adjusting stiffness but do not consider changes in permeability. However, to the author's best knowledge, only PM4Sand can precisely anticipate the ultimate post-liquefaction settlement by considering both liquefaction triggering and reconsolidation behavior.

- Although the prediction accuracy of the dissipation rates from the present study differed from the rates observed in the experiment, PM4Sand was able to capture the excess pore pressure generation from the experiment (Thevanayagam et al. 2009).
- The parametric analysis with 12 different ground motions shows that the stone columns are efficient under real ground conditions in terms of mitigating post-liquefaction settlement. The rate of excess pore pressure dissipation increased for all ground motions. These results underscore the practical significance of implementing effective ground improvement measures like stone columns to ensure the longevity and safety of structures in earthquake-prone areas.
- Analyzing the new proposed model with stone columns from Phase I, it can be inferred that the stabilizing effect of stone columns (because of e.g., improved stiffness) plays a pivotal role in influencing settlement behavior during and after seismic events. In addition, the dissipation of excess pore pressure contributes to maintaining a relatively low excess pore pressure ratio.
- The inclusion of stone columns from Phase III showed the efficacy of stone columns after the liquefaction triggering of natural ground. The final post-liquefaction settlement was reduced to some extent in this case.
- Activating the PostShake factor significantly increased the post-liquefaction settlement. This outcome highlights the critical influence of the PostShake factor (i.e., using constitutive models that particularly account for reconsolidation settlement) on the settlement dynamics, shedding light on its crucial role in capturing the post-liquefaction response within the analyzed model.
- To model the effect of stone columns in real field conditions, a footing load was applied on top of the proposed numerical model. The stone columns mitigated the post-liquefaction settlement by 10 folds, primarily due to limiting increases in pore pressure ratio during the seismic loading. This shows the effectiveness of stone columns in enhancing the resilience of the soil-structure system.

5.2 Limitations and Recommendations

One of the limitations of this study is that it did not consider changes in hydraulic conductivity (k) throughout the simulation. Therefore, to better capture the time rate of settlement, the effect of having a variable k should be considered and assessed. Nevertheless, in this case, constant k was assumed as the study mainly focused on the prediction of the magnitude of final settlement. Moreover, this study does not explicitly include the calibration of the constitutive model. A soil-specific calibration of reconsolidation behavior might be required to enhance the agreement of numerical analysis and experiments.

The efficacy of stone columns in enhancing the geotechnical response to earthquake loading has been verified using Plaxis 2D within the PM4Sand framework. However, this study has not conducted an optimization analysis to determine the required number of stone columns. The optimization study is imperative for the simulation of real scenarios like embankments, settlement of structures, and so on to ensure cost-effective and efficient solutions. Additionally, this paper does not encompass the parametric analyses involving variations of stone column parameters such as diameter, spacing, and stiffness. It is essential to carry out a sensitivity analysis by varying these parameters, which provide a basis for the optimal design of stone columns.

The study does not consider crucial effects during the installation of stone columns, such as the densification around the stone columns and the increase in the lateral earth pressure coefficient. Incorporating these variations in soil conditions is important to better and more accurately determine the mechanisms that make stone columns a valid ground reinforcement method when subjected to ground motions, liquefaction, and reconsolidation. Additionally, this study does not consider the effect of clogging on the rate of consolidation of the stone column-improved ground by particle migration.

The study is limited to 2D plane-strain conditions. Further analysis should be performed to assess and better comprehend 3D effects on the performance of stone columns. Likewise, further studies should augment the dataset of ground motions beyond the 12 earthquakes considered in this study. A detailed investigation of ground motions characterized by diverse ranges of Intensity Measures (predominant frequency, peak ground velocity, peak ground displacement) would significantly contribute to an improved understanding of the dynamics influencing the post-liquefaction settlement.

Furthermore, an extensive study on settlement behavior under foundation loading subjected to a diversified set of input motions is recommended. Additionally, a thorough exploration of various footing conditions, including the examination of different depths of embedment and variations in load magnitudes, is suggested. Finally, additional experimental and numerical investigations are required to increase the accuracy of numerical predictions in terms of reconsolidation settlement induced by liquefaction in both natural and reinforced ground conditions.

References

Adalier, K., A. Elgamal, J. Meneses, and J. I. Baez. 2003. "Stone columns as liquefaction countermeasure in non-plastic silty soils." *Soil Dynamics and Earthquake Engineering*, 23 (7): 571–584. https://doi.org/10.1016/S0267-7261(03)00070-8.

Adamidis, O., and G. S. P. Madabhushi. 2016. "Post-liquefaction reconsolidation of sand." *Proceedings of the Royal Society A: Mathematical, Physical and Engineering Sciences*, 472 (2186): 20150745. https://doi.org/10.1098/rspa.2015.0745.

Alexander, G. J., J. Arefi, L. M. Wotherspoon, A. C. Stolte, B. R. Cox, R. A. Green, and C. M. Wood. 2019. "A case study of stone column ground improvement performance during a sequence of seismic events." *In Proc., 7th Int. Conf. on Earthquake Geotechnical Engineering (7ICEGE)*. London: CRC Press.

Ancheta, T. D., R. B. Darragh, J. P. Stewart, E. Seyhan, W. J. Silva, B. S.-J. Chiou, K. E. Wooddell, R. W. Graves, A. R. Kottke, and D. M. Boore. 2014. "NGA-West2 database." *Earthquake Spectra*, 30 (3): 989–1005. SAGE Publications Sage UK: London, England.

Andrianopoulos, K. I., A. G. Papadimitriou, and G. D. Bouckovalas. 2010. "Bounding surface plasticity model for the seismic liquefaction analysis of geostructures." *Soil Dynamics and Earthquake Engineering*, 30 (10): 895–911. https://doi.org/10.1016/j.soildyn.2010.04.001.

Arboleda-Monsalve, L. G., J. A. Mercado, A. Sover, and D. G. Zapata-Medina. 2017. "Liquefaction analyses of the Port of Long Beach using the UBC3D-PLM constitutive soil model." *In Geotechnical Frontiers 2017: Seismic Performance and Liquefaction, Geotechnical Special Publication 281, edited by T. L. Brandon and R. J. Valentine*, 369–378. Reston, VA: ASCE.

Armstrong, R. J., R. W. Boulanger, and M. H. Beaty. 2013. "Liquefaction Effects on Piled Bridge Abutments: Centrifuge Tests and Numerical Analyses." *Journal of Geotechnical and Geoenvironmental Engineering*, 139 (3): 433–443. https://doi.org/10.1061/(ASCE)GT.1943-5606.0000780.

Asgari, A., M. Oliaei, and M. Bagheri. 2013. "Numerical simulation of improvement of a liquefiable soil layer using stone column and pile-pinning techniques." *Soil Dynamics and Earthquake Engineering*, 51: 77–96. https://doi.org/10.1016/j.soildyn.2013.04.006.

Badanagki, M., S. Dashti, and P. Kirkwood. 2018. "Influence of Dense Granular Columns on the Performance of Level and Gently Sloping Liquefiable Sites." *Journal of Geotechnical and Geoenvironmental Engineering*, 144 (9). https://doi.org/10.1061/(ASCE)GT.1943-5606.0001937.

Basu, D., J. Montgomery, and A. W. Stuedlein. 2022. "Observations and challenges in simulating post-liquefaction settlements from centrifuge and shake table tests." *Soil Dynamics and Earthquake Engineering*, 153: 107089. https://doi.org/10.1016/j.soildyn.2021.107089.

Beaty, M., and P. M. Byrne. 1998. "An effective stress model for pedicting liquefaction behaviour of sand." *In Vol. 1 of Geotechnical Earthquake Engineering and Soil Dynamics III*, 766–777. Reston, VA: ASCE.

Beaty, M. H. 2001. "A synthesized approach for estimating liquefaction-induced displacements of geotechnical structures." Ph.D. thesis, The University of British Columbia. Vancouver, B.C.

Beaty, M. H., and P. M. Byrne. 2011. "UBCSAND constitutive model version 904aR." *Documentation Rep., UBCSAND Constitutive Model on Itasca UDM Website*.

Bhochhibhoya, S., R. Maharjan, R. Adhikari, S. Gurung, P. Adhikari, S. Shrestha, and M. S. K. C. 2023. "Suitability Assessment of Stone Columns to Improve Soil Foundation in Kathmandu Valley, Nepal." *Geotechnical and Geological Engineering*, 41 (1): 57–73. https://doi.org/10.1007/s10706-022-02262-y.

Boulanger, R. W., and I. M. Idriss. 2014. "CPT and SPT based liquefaction triggering procedures." *Report No. UCD/CGM.-14/01, April. Davis, CA: University of California at Davis.*

Boulanger, R. W., M. Khosravi, A. Khosravi, and D. W. Wilson. 2018. "Remediation of liquefaction effects for an embankment using soil-cement walls: Centrifuge and numerical modeling." *Soil Dynamics and Earthquake Engineering*, 114: 38–50. https://doi.org/10.1016/j.soildyn.2018.07.001.

Boulanger, R. W., and K. Ziotopoulou. 2015. "PM4Sand (Version 3): A sand plasticity model for earthquake engineering applications." California: Center for Geotechnical Modeling Report No. UCD/CGM-15/01, Department of Civil and Environmental Engineering, University of California At Davis.

Bray, J. D., and J. Macedo. 2017. "6th Ishihara lecture: Simplified procedure for estimating liquefaction-induced building settlement." *Soil Dynamics and Earthquake Engineering*, 102: 215–231. https://doi.org/10.1016/j.soildyn.2017.08.026.

Brennan, A., and S. Madabhushi. 2011. "Measurement of coefficient of consolidation during reconsolidation of liquefied sand." *Geotechnical Testing Journal*, 34 (2): 139–146. ASTM International.

Byrne, P. M., S.-S. Park, M. Beaty, M. Sharp, L. Gonzalez, and T. Abdoun. 2004. "Numerical modeling of liquefaction and comparison with centrifuge tests." *Canadian Geotechnical Journal*, 41 (2): 193–211. https://doi.org/10.1139/t03-088.

Cascone, E., G. Biondi, D. Aliberti, and S. Rampello. 2021. "Effect of vertical input motion and excess pore pressures on the seismic performance of a zoned dam." *Soil Dynamics and Earthquake Engineering*, 142: 106566. https://doi.org/10.1016/j.soildyn.2020.106566.

Cetin, K. O., R. B. Seed, A. Der Kiureghian, K. Tokimatsu, L. F. Harder, R. E. Kayen, and R. E. S. Moss. 2004. "Standard Penetration Test-Based Probabilistic and Deterministic Assessment of Seismic Soil Liquefaction Potential." *Journal of Geotechnical and Geoenvironmental Engineering*, 130 (12): 1314–1340. https://doi.org/10.1061/(ASCE)1090-0241(2004)130:12(1314).

Chakraborty, A., and V. A. Sawant. 2022. "Numerical Simulation of Earthen Embankment Resting on Liquefiable Soil and Remediation Using Stone Columns." *International Journal of Geomechanics*, 22 (11). https://doi.org/10.1061/(ASCE)GM.1943-5622.0002559.

Chen, L. 2020. "Implementation, verification, validation, and application of two constitutive models for earthquake engineering applications." Ph.D. thesis. Seattle, WA: University of Washington.

Clemente, J. L. M., H. Senapathy, and J. R. Davie. 2005. "Performance prediction of stone-column-supported foundations." *Proceedings of the 16th International Conference on Soil Mechanics and Geotechnical Engineering*, 1327–1330. IOS Press.

Cubrinovski, M., J. D. Bray, C. de la Torre, M. Olsen, B. Bradley, G. Chiaro, E. Stocks, L. Wotherspoon, and T. Krall. 2018. "Liquefaction-Induced Damage and CPT Characterization of the Reclamations at CentrePort, Wellington." *Bulletin of the Seismological Society of America*, 108 (3B): 1695–1708. https://doi.org/10.1785/0120170246.

Dafalias, Y. F., and M. T. Manzari. 2004. "Simple Plasticity Sand Model Accounting for Fabric Change Effects." *J Eng Mech*, 130 (6): 622–634. https://doi.org/10.1061/(ASCE)0733-9399(2004)130:6(622).

Diaz-Segura, E. G. 2015. "Assessment of Liquefaction Triggering: the UBC3D-PLM Constitutive Model Versus Semi–Empirical Methods Based on SPT-N Values." *Electronic Journal of Geotechnical Engineering*, 20 (18): 10061–10071.

Dobry, R., S. Thevanayagam, C. Medina, R. Bethapudi, A. Elgamal, V. Bennett, T. Abdoun, M. Zeghal, U. El Shamy, and V. M. Mercado. 2011. "Mechanics of Lateral Spreading Observed in a Full-Scale Shake Test." *Journal of Geotechnical and Geoenvironmental Engineering*, 137 (2): 115–129. https://doi.org/10.1061/(ASCE)GT.1943-5606.0000409.

Ecemis, N. 2021. "Experimental and numerical modeling on the liquefaction potential and ground settlement of silt-interlayered stratified sands." *Soil Dynamics and Earthquake Engineering*, 144: 106691. https://doi.org/10.1016/j.soildyn.2021.106691.

Elgamal, A., Z. Yang, E. Parra, and A. Ragheb. 2003. "Modeling of cyclic mobility in saturated cohesionless soils." *Int J Plast*, 19 (6): 883–905. https://doi.org/10.1016/S0749-6419(02)00010-4.

Finn, W. D. L., G. R. Martin, and P. M. Byrne. 1976. "Seismic Response and Liquefaction of Sands." *Journal of the Geotechnical Engineering Division*, 102 (8): 841–856. https://doi.org/10.1061/AJGEB6.0000310.

Florin, V. A. 1961. "Liquefaction of saturated sandy soils." *Proc. of the 5th international conference on soil mechanics and foundation engineering*, 107–111.

Gingery, J. R. 2019. "Modeling reinforcing effects of ground improvement in mitigating seismic settlement." *Earthquake Geotechnical Engineering for Protection and Development of Environment and Constructions*, 2651–2658. CRC Press.

Goren, L., E. Aharonov, D. Sparks, and R. Toussaint. 2010. "Pore pressure evolution in deforming granular material: A general formulation and the infinitely stiff approximation." *J Geophys Res*, 115 (B9): B09216. https://doi.org/10.1029/2009JB007191.

Green, , Russell A., C. G. Olgun, and K. J. Wissmann. 2008. "Shear Stress Redistribution as a Mechanism to Mitigate the Risk of Liquefaction." *Geotechnical Earthquake Engineering and Soil Dynamics IV*, 1–10. Reston, VA: ASCE.

Green, R. A., and J. J. Bommer. 2019. "What is the Smallest Earthquake Magnitude that Needs to be Considered in Assessing Liquefaction Hazard?" *Earthquake Spectra*, 35 (3): 1441–1464. https://doi.org/10.1193/032218EQS064M.

Green, R. A., M. Cubrinovski, B. Cox, C. Wood, L. Wotherspoon, B. Bradley, and B. Maurer. 2014. "Select Liquefaction Case Histories from the 2010–2011 Canterbury Earthquake Sequence." *Earthquake Spectra*, 30 (1): 131–153. https://doi.org/10.1193/030713EQS066M.

Green, R. A., C. Wood, B. Cox, M. Cubrinovski, L. Wotherspoon, B. Bradley, T. Algie, J. Allen, A. Bradshaw, and G. Rix. 2011. "Use of DCP and SASW tests to evaluate liquefaction potential: Predictions vs. observations during the recent New Zealand earthquakes." *Seismological Research Letters*, 82 (6): 927–938. Seismological Society of America.

Huang, D., and G. Wang. 2017. "Energy-compatible and spectrum-compatible (ECSC) ground motion simulation using wavelet packets." *Earthq Eng Struct Dyn*, 46 (11): 1855–1873. https://doi.org/10.1002/eqe.2887.

Iai, S., K. Koizumi, S. Noda, and H. Tsuchida. 1988. "Large Scale Model Tests and Analyses of Gravel Drains." *Proc., 9th World Conf. on Earthquake Engineering, Vol. III*. Tokyo, Japan: Japan Association for Earthquake Disaster Prevention.

Idriss, I. M., and R. W. Boulanger. 2007. "SPT- and CPT-Based Relationships for The Residual Shear Strength of Liquefied Soils." *Proc., 4th Int. Conf. on Earthquake Geotechnical Engineering*, 1–22. New York: Springer.

Ishihara, K., K. Harada, W. F. Lee, C. C. Chan, and A. M. M. Safiullah. 2016. "Post-liquefaction settlement analyses based on the volume change characteristics of undisturbed and reconstituted samples." *Soils and Foundations*, 56 (3): 533–546. https://doi.org/10.1016/j.sandf.2016.04.019.

Ishihara, K., and M. Yoshimine. 1992. "Evaluation of Settlements in Sand Deposits Following Liquefaction During Earthquakes." *Soils and Foundations*, 32 (1): 173–188. https://doi.org/10.3208/sandf1972.32.173.

Itasca Consulting Group, Inc. . 2016. "FLAC - fast Lagrangian analysis of continua, Ver.8.0." *Itasca, Minneapolis*.

Jamiolkowski, M., D. C. F. Lo Presti, and M. Manassero. 2003. "Evaluation of Relative Density and Shear Strength of Sands from CPT and DMT." *Soil Behavior and Soft Ground Construction*, 201–238. Reston, VA: ASCE.

Jiang, Y., R. A. Green, and O.-D. Taylor. 2021. "Expanded Byrne model for evaluating seismic compression." *Earthquake Spectra*, 37 (2): 612–636. https://doi.org/10.1177/8755293020957350.

Ju, L., and D. Vassalos. 2015. "Potential assessment of cargo liquefaction based on an UBC3D-PLM model." *12th International Conference on the Stability of Ships and Ocean Vehicles (STAB 2015)*, 1123–1131.

Kamai, R., and R. W. Boulanger. 2013. "Simulations of a Centrifuge Test with Lateral Spreading and Void Redistribution Effects." *Journal of Geotechnical and Geoenvironmental Engineering*, 139 (8): 1250–1261. https://doi.org/10.1061/(ASCE)GT.1943-5606.0000845.

Kim, S.-R., J.-I. Hwang, H.-Y. Ko, and M.-M. Kim. 2009. "Development of Dissipation Model of Excess Pore Pressure in Liquefied Sandy Ground." *Journal of Geotechnical and Geoenvironmental Engineering*, 135 (4): 544–554. https://doi.org/10.1061/(ASCE)1090-0241(2009)135:4(544).

Kirsch, K. 2010. "Ground Improvement by Deep Vibratory Methods." *Noise Control Eng J*, 58 (6). https://doi.org/10.3397/1.3511778.

Kramer, S. L. 1996. *Geotechnical earthquake engineering*. Prentice-Hall, Englewood Cliffs, N. J., 653.

Kramer, S. L., and H. B. Seed. 1988. "Initiation of Soil Liquefaction Under Static Loading Conditions." *Journal of Geotechnical Engineering*, 114 (4): 412–430. https://doi.org/10.1061/(ASCE)0733-9410(1988)114:4(412).

Kramer, S. L., and C.-H. Wang. 2015. "Empirical Model for Estimation of the Residual Strength of Liquefied Soil." *Journal of Geotechnical and Geoenvironmental Engineering*, 141 (9). https://doi.org/10.1061/(ASCE)GT.1943-5606.0001317.

Lambe, P. C., and R. V. Whitman. 1985. "Dynamic Centrifugal Modeling of a Horizontal Dry Sand Layer." *Journal of Geotechnical Engineering*, 111 (3): 265–287. https://doi.org/10.1061/(ASCE)0733-9410(1985)111:3(265).

Li, P., S. Dashti, M. Badanagki, and P. Kirkwood. 2018. "Evaluating 2D numerical simulations of granular columns in level and gently sloping liquefiable sites using centrifuge experiments." *Soil Dynamics and Earthquake Engineering*, 110: 232–243. https://doi.org/10.1016/j.soildyn.2018.03.023.

Makra, A. 2013. "Evaluation of the UBC3D-PLM constitutive model for prediction of earthquake induced liquefaction on embankment dams." Master's Thesis. Delft, The Netherlands: Delft University of Technology.

Martin, J. B. G., and G. R. Martin. 1992. "Quantitative evaluation of stone column techniques for earthquake liquefaction mitigation." *Proceedings of the tenth world conference on earthquake engineering*, 19–24.

McCabe, B. A., G. J. Nimmons, and D. Egan. 2009. "A review of field performance of stone columns in soft soils." *Proceedings of the Institution of Civil Engineers - Geotechnical Engineering*, 162 (6): 323–334. https://doi.org/10.1680/geng.2009.162.6.323.

Mehrzad, B., Y. Jafarian, C. J. Lee, and A. H. Haddad. 2018. "Centrifuge study into the effect of liquefaction extent on permanent settlement and seismic response of shallow foundations." *Soils and Foundations*, 58 (1): 228–240. https://doi.org/10.1016/j.sandf.2017.12.006.

NASEM (National Academies of Sciences and Medicine). 2016. "State of the art and practice in the assessment of earthquake-induced soil liquefaction and its consequences." Washington, DC: National Academies Press.

Nicholson, P. G. 2014. *Soil improvement and ground modification methods*. Oxford, UK: Butterworth-Heinemann.

Olson, S. M., and T. D. Stark. 2002. "Liquefied strength ratio from liquefaction flow failure case histories." *Canadian Geotechnical Journal*, 39 (3): 629–647. https://doi.org/10.1139/t02-001.

Petalas, A., and V. Galavi. 2013. "Plaxis liquefaction model UBC3D-PLM." Delft, Netherlands: PLAXIS B.V.

Plaxis. 2018. "Plaxis 2D reference manual." *Delft Univ. of Technology and Plaxis, Delft, Netherlands*.

Poorooshasb, H. B., and G. G. Meyerhof. 1997. "Analysis of behavior of stone columns and lime columns." *Comput Geotech*, 20 (1): 47–70. https://doi.org/10.1016/S0266-352X(96)00013-4.

Prevost, J. H. 1985. "A simple plasticity theory for frictional cohesionless soils." *International Journal of Soil Dynamics and Earthquake Engineering*, 4 (1): 9–17. https://doi.org/10.1016/0261-7277(85)90030-0.

Puebla, H., P. M. Byrne, and R. Phillips. 1997. "Analysis of CANLEX liquefaction embankments: prototype and centrifuge models." *Canadian Geotechnical Journal*, 34 (5): 641–657. https://doi.org/10.1139/t97-034.

Quevedo, H. 2019. "Seismic liquefaction analysis of a critical facility with PM4Sand in Plaxis." MSc Thesis. Delft, The Netherlands: Delft University of Technology.

Ramirez, J., A. R. Barrero, L. Chen, S. Dashti, A. Ghofrani, M. Taiebat, and P. Arduino. 2018. "Site Response in a Layered Liquefiable Deposit: Evaluation of Different Numerical Tools and Methodologies with Centrifuge Experimental Results." *Journal of Geotechnical and Geoenvironmental Engineering*, 144 (10). https://doi.org/10.1061/(ASCE)GT.1943-5606.0001947.

Rashidian, V., and L. G. Baise. 2020. "Regional efficacy of a global geospatial liquefaction model." *Eng Geol*, 272: 105644. https://doi.org/10.1016/j.enggeo.2020.105644.

Schmertmann, J. H. 1976. "An updated correlation between relative density DR and Fugro-type electric cone bearing, qc." *Contract report DACW*, 39–76.

Schofield, A. N., and P. Wroth. 1968. *Critical state soil mechanics*. McGraw-hill London.

Scott, R. F. 1986. "Solidification and Consolidation of a Liquefied Sand Column." *Soils and Foundations*, 26 (4): 23–31. https://doi.org/10.3208/sandf1972.26.4_23.

Seed, H. B., I. M. Idriss, and I. Arango. 1983. "Evaluation of Liquefaction Potential Using Field Performance Data." *Journal of Geotechnical Engineering*, 109 (3): 458–482. https://doi.org/10.1061/(ASCE)0733-9410(1983)109:3(458).

Seed, R. B., K. O. Cetin, R. E. S. Moss, A. M. Kammerer, J. Wu, J. M. Pestana, and M. F. Riemer. 2001. "Recent advances in soil liquefaction engineering and seismic site response evaluation." *4th Int. Conf. Recent Advanced in Geotechnical Earthquake Engineering and soil dinamics, San Diego, California*.

Seed, R. B., K. O. Cetin, R. E. S. Moss, A. M. Kammerer, J. Wu, J. M. Pestana, M. Riemer, R. B. Sancio, J. D. Bray, R. E. Kayen, and A. T. Faris. 2003. "Recent Advances in Soil Liquefaction Engineering: A Unified and Consistent Framework." *EERC-2003–06, Earthquake Engineering Research Institute*. Berkeley, Calif.

Seed, R. B., and L. F. Harder Jr. 1990. "SPT-based Analysis of Cyclic Pore Pressure Generation and Undrained Residual Strength." *Proc., H.B. Seed Memorial Symp., Vol. 2*, 351–376. Vancouver, BC, Canada: BiTech Publishing.

Stark, T. D., and G. Mesri. 1992. "Undrained Shear Strength of Liquefied Sands for Stability Analysis." *Journal of Geotechnical Engineering*, 118 (11): 1727–1747. https://doi.org/10.1061/(ASCE)0733-9410(1992)118:11(1727).

Suits, L. D., T. C. Sheahan, S. Thevanayagam, T. Kanagalingam, A. Reinhorn, R. Tharmendhira, R. Dobry, M. Pitman, T. Abdoun, A. Elgamal, M. Zeghal, N. Ecemis, and U. El Shamy. 2009. "Laminar Box System for 1-g Physical Modeling of Liquefaction and Lateral Spreading." *Geotechnical Testing Journal*, 32 (5): 102154. https://doi.org/10.1520/GTJ102154.

Taiebat, M., and Y. F. Dafalias. 2008. "SANISAND: Simple anisotropic sand plasticity model." *Int J Numer Anal Methods Geomech*, 32 (8): 915–948. https://doi.org/10.1002/nag.651.

Terzaghi, R. D. 1965. "Sources of error in joint surveys." *Geotechnique*, 15 (3): 287–304. Thomas Telford Ltd.

Thevanayagam, S., R. Nashed, and G. R. Martin. 2009. "Dynamic compaction of saturated sands and silty sands: theory." *Proceedings of the Institution of Civil Engineers - Ground Improvement*, 162 (2): 57–68. https://doi.org/10.1680/grim.2009.162.2.57.

Thum, T. S., A. Yerro, A. Saade, E. Ye, K. J. Wissmann, and R. A. Green. 2022. "Numerical modelling of rammed aggregate piers (RAP) in liquefiable soil." *Soil Dynamics and Earthquake Engineering*, 153: 107088. https://doi.org/10.1016/j.soildyn.2021.107088.

Tokimatsu, K., and H. B. Seed. 1987. "Evaluation of settlements in sands due to earthquake shaking." *Journal of geotechnical engineering*, 113 (8): 861–878. American Society of Civil Engineers.

Toloza, P. 2018. "Liquefaction modelling using the PM4Sand constitutive model in Plaxis 2D." *Delft University of Technology*.

Vilhar, G., A. Laera, F. Foria, A. Gupta, and R. B. J. Brinkgreve. 2018. "Implementation, Validation, and Application of PM4Sand Model in PLAXIS." *Geotechnical Earthquake Engineering and Soil Dynamics V*, 200–211. Reston, VA: American Society of Civil Engineers.

Wang, G. 2012. "Efficiency of scalar and vector intensity measures for seismic slope displacements." *Frontiers of Structural and Civil Engineering*, 6 (1): 44–52. https://doi.org/10.1007/s11709-012-0138-x.

Wang, G., and Y. Xie. 2014. "Modified Bounding Surface Hypoplasticity Model for Sands under Cyclic Loading." *J Eng Mech*, 140 (1): 91–101. https://doi.org/10.1061/(ASCE)EM.1943-7889.0000654.

Wang, Z., Y. F. Dafalias, and C. Shen. 1990. "Bounding Surface Hypoplasticity Model for Sand." *J Eng Mech*, 116 (5): 983–1001. https://doi.org/10.1061/(ASCE)0733-9399(1990)116:5(983).

Wood, D. M. 1990. *Soil behaviour and critical state soil mechanics*. New York: Cambridge University Press.

Wu, J., and R. B. Seed. 2004. "Estimation of liquefaction-induced ground settlement (case studies)." University of Missouri--Rolla.

Yang, M., M. Taiebat, and Y. F. Dafalias. 2022. "SANISAND-MSf: a sand plasticity model with memory surface and semifluidised state." *Géotechnique*, 72 (3): 227–246. https://doi.org/10.1680/jgeot.19.P.363.

Zeybek, A., and G. S. P. Madabhushi. 2023. "Assessment of soil parameters during post-liquefaction reconsolidation of loose sand." *Soil Dynamics and Earthquake Engineering*, 164: 107611. https://doi.org/10.1016/j.soildyn.2022.107611.

Zhang, G., P. K. Robertson, and R. W. I. Brachman. 2002. "Estimating liquefaction-induced ground settlements from CPT for level ground." *Canadian Geotechnical Journal*, 39 (5): 1168–1180. https://doi.org/10.1139/t02-047.

Zhang, J., W. H. Tang, and L. M. Zhang. 2010. "Efficient Probabilistic Back-Analysis of Slope Stability Model Parameters." *Journal of Geotechnical and Geoenvironmental Engineering*, 136 (1): 99–109. https://doi.org/10.1061/(ASCE)GT.1943-5606.0000205.

Zhou, Y.-G., K. Liu, Z.-B. Sun, and Y.-M. Chen. 2021. "Liquefaction mitigation mechanisms of stone column-improved ground by dynamic centrifuge model tests." *Soil Dynamics and Earthquake Engineering*, 150: 106946. https://doi.org/10.1016/j.soildyn.2021.106946.

Ziotopoulou, K., and R. W. Boulanger. 2013. "Numerical modeling issues in predicting post-liquefaction reconsolidation strains and settlements." *Proc., 10th Int. Conf. on Urban Earthquake Engineering*, 469–475. Tokyo Institute of Technology.

Ziotopoulou, K., and J. Montgomery. 2017. "Numerical modeling of earthquake-induced liquefaction effects on shallow foundations." *Proceedings of 16th world conference on earthquake engineering*.